Nano Today 45 (2022) 101513

Contents lists available at ScienceDirect

Nano Today

journal homepage: www.elsevier.com/locate/nanotoday

Review

Recentadvances on biomechanical motion-driven triboelectric nanogenerators for drug delivery

Partho Adhikary[a,1], M. A. Parvez Mahmud[b,*,2], Tahsin Solaiman[a,3], Zhong Lin Wang[c,*,4]

[a] Department of Biomedical Engineering, Khulna University of Engineering & Technology, Khulna 9203, Bangladesh
[b] School of Engineering, Deakin University, Geelong, Victoria 3216, Australia
[c] School of Material Science and Engineering, Georgia Institute of Technology, Atlanta, GA 30332-0245, USA

ARTICLE INFO

Article history:
Received 1 November 2021
Received in revised form 15 May 2022
Accepted 27 May 2022
Available online xxxx

Keywords:
Triboelectric nanogenerator
Biomechanical energy harvesting
Transdermal drug delivery
Self-powered drug delivery
Stimuli-responsive biopolymer
On-demand drug delivery

ABSTRACT

In recent years, unprecedented advances are noticed in wearable sensors and therapeutic devices because of their portability, low power consumption, m-health solution, and self-administration phenomena. A triboelectric nanogenerator (TENG) converts biomechanical energy into electricity through the combined effects of triboelectrification and electrostatic induction, gaining ubiquitous attention because of its sensing and energy harvesting properties. Nano carriers like stimuli-responsive biopolymers, nanoparticles, microneedles, and liposomes are the most frequently used drug delivery vehicle in invasive as well as transdermal drug delivery (TDD) system that is stimulated and controlled by TENGs power supply. Hence, biomaterials and organelles are exploited in drug delivery systems along with TENG to achieve a site-specific controlled drug release. With the progress of biomechanical energy harvesting, self-power drug delivery has been proven to be a worthy substitute for oral or injectable drug delivery with high performance and therapeutic accuracy. Continuous power generation, sustainability, and precise functionality of self-powered devices and wearable sensors have still encountered some hitches during biomedical applications. This focused review will summarize the recent developments of TENG-powered drug delivery systems. An in-depth explanation of current challenges and future directions to ensure precise and on-demand drug delivery will also be elucidated lucidly.

Contents

* Corresponding authors.
E-mail addresses: parthoadhikary2k14@gmail.com (P. Adhikary), m.a.mahmud@deakin.edu.au (M.A.P. Mahmud), tahsinsohan@gmail.com (T. Solaiman), zhong.wang@mse.gatech.edu (Z.L. Wang).
[1] ORCID id: https://orcid.org/0000-0002-7088-5604
[2] ORCID id: https://orcid.org/0000-0002-1905-6800
[3] ORCID id: https://orcid.org/0000-0002-4370-9373
[4] ORCID id: https://orcid.org/0000-0002-5530-0380

https://doi.org/10.1016/j.nantod.2022.101513
1748-0132/

Introduction

The development and advances of tiny, smart devices have gained a tremendous attraction for self-monitoring, health care systems, and therapeutics nowadays. Since the uses of IoT based health care, artificial intelligence (AI), and wearable devices are expanding rapidly and big data, deep learning, and AI implement in biomedical applications highly depend on sensor networks that require an uninterrupted power supply, TENG would be a principal part to generate the desired power to fulfil this demand. TENG, using the combination of contact electrification (CE) and electrostatic induction can harvest biomechanical energy from human locomotion and transform it into electricity [1]. Based on the operation mode, TENG can convert 50–85% environmental and biomechanical energy paving the way to use it as an energy harvester [2]. The TENG can supply steady voltage to drug release devices [3]. Thus TENG ameliorates the previous inconvenience of bulky power storage devices and feedback-controlled components when treating dermal analgesia or local sweat induction-like diseases [4,5].

Some prolific scientists are trying to employ these real-time energy harvesting phenomena in embedded drug delivery systems in modern healthcare technology. In clinical practice, on-demand embedded drug delivery refers to a controllable drug release that supports patients with various indications and allows them to govern the individual location, measured quantity, rate or duration of dosages, and drug release efficacy [6]. Wearable and implantable site-specific drug delivery ensure high efficacy with improving outcomes and low side effects with overall therapeutic costs reduction. Films (patches) and gels are considered a boon in TDD to treat skin diseases and wound healing over the past decades [7–14]. Films (patches) are used as a drug reservoir with adhesiveness properties, thorough performance at the targeted site, and prolonged drug release with therapeutic perfections [15–18]. A wide range of trigger-able biopolymers that can be galvanized by endogenous (e.g. enzyme, glucose, pH) or exogenous (e.g. light, ultrasound, electric-field) means make controllable drug release a feasible method of treatment at present time [19]. Endogenous stimulus depends on individual physiological conditions, and it's quite difficult to ensure precise trigger and control over delivery rates. In addition, carrier-based delivery using exogenous stimuli provides more freedom than endogenous one. Thus TENG powered stimuli-based drug delivery solves the prior uncertainty of endogenous stimulations.

TENG-based TDD used electroporation (EP), which requires a high voltage electrical pulse (up to 1000 V) to the skin to create transient pores in plasma membranes which are essential for biomolecules to reach into the cells [20,21]. Electroporation is the method of transferring DNA into the cells by exposure to a rapid pulse with high voltage. Whereas, electrophoresis is the method of separation of molecules based on their electric charge. With the assistance of electrophoresis, charge molecules can drive through the skin after applying a current of ˂ 0.50 mA per centimetre square area [22]. During electrophoresis separation/migration of drug molecules occurs under an electric field and electrodes (anode, cathode) are connected by a conducting medium (electrolyte) collectively known as the electrophoretic system. Migration/separation occurs due to the varying velocity of charge molecules that is the product of particle mobility and electric field strength. Electrical parameters (current, voltage, power) and chemical factors (pH value, ionic strength, pore size, and viscosity) are the most influential factors in an electrophoretic system. The TDD system uses the iontophoresis principle to transport hydrophilic and/or charge molecules across the skin that is powered by TENG [23–25]. Voltage-controlled organic electronic ion pumps release both small charge particle/biochemical ions as well as large protein molecules and thus facilitate on-demand drug delivery [26–28]. There is a precedent that TDD amounts of fentanyl, timolol [29,30], salmon calcitonin, parathyroid hormone [29,31,32], DNA [29,33], and fluorescein iso-thiocyanate-dextrans [29,34] have been increased at a notable rate by using EP. Results showed that electrically stimulated drug carriers could release drugs of 3 $\mu g/cm^2$ upon 1.5 min of hand rotation [35]. Moreover, it is also possible to control drug discharge levels by tuning the TENG maneuver time or resistance of the power management circuit from 0.05 $\mu g/cm^2$ to 0.25 $\mu g/cm^2$ per minute [35]. The electric field generated by TENG in drug delivery mechanisms plays dual roles to create pores in the skin and provide the local driving forces for the hydrophilic molecules' transportation [36]. Despite having myriad applications in cell modulation, microbial disinfection, IoT based health monitoring, and biodegradable electronics, TENG still possesses some challenges in encapsulation, implantation and biocompatibility that must be attained. An effective correction of these inconveniences can lead to TENG driven drug delivery a key medium for future medicine and therapeutics.

The central theme of this review will convey three integral parts of the TENG-related drug delivery system that remained untouched under huge loads of existing research. First, the fundamental concept of TENG-based embedded drug delivery will be summarized in the earlier section. Secondly, current challenges assuming in TENG technology that hobble its currency in drug delivery will be discussed. Finally, we will expound on the future direction that makes TENG-driven drug delivery commercially fit as a candidate for health care and patient monitoring.

Working mechanism of triboelectric nano-generator

Triboelectric Nanogenerator (TENG) uses the coupling effect of triboelectricity (TE) and electric induction that was developed by Wang et al. in 2012 [37]. Although it was an ancient process used more than two thousand years ago, the fundamental understanding was perceptible in 2019 [38]. TENG's basic operation is simply described as a combination of two materials disjointed by a gap that behaves like a capacitor. Its capacitance can vary according to Maxwell's displacement current [39,40]. In 2017, Wang et al. gave a comprehensive theoretical calculation and origin of electricity between two dielectric materials [41]. When it was studied at the nanoscale, it became fathomable that the electron transfer mechanism is governing in TE [42]. To understand the foundation of triboelectricity, Wang and Wang [1] suggested the interatomic interaction model clarifies TE on a submicroscopic level, in which triboelectrification occurs between two particles with partial overlay in their micro/nano-electronic clouds or wave functions [38]. The interaction of two atoms and their interatomic distance is shown in Fig. 1A(i-ii). The author showed that partial overlap was established between two atoms when an external compressive force was

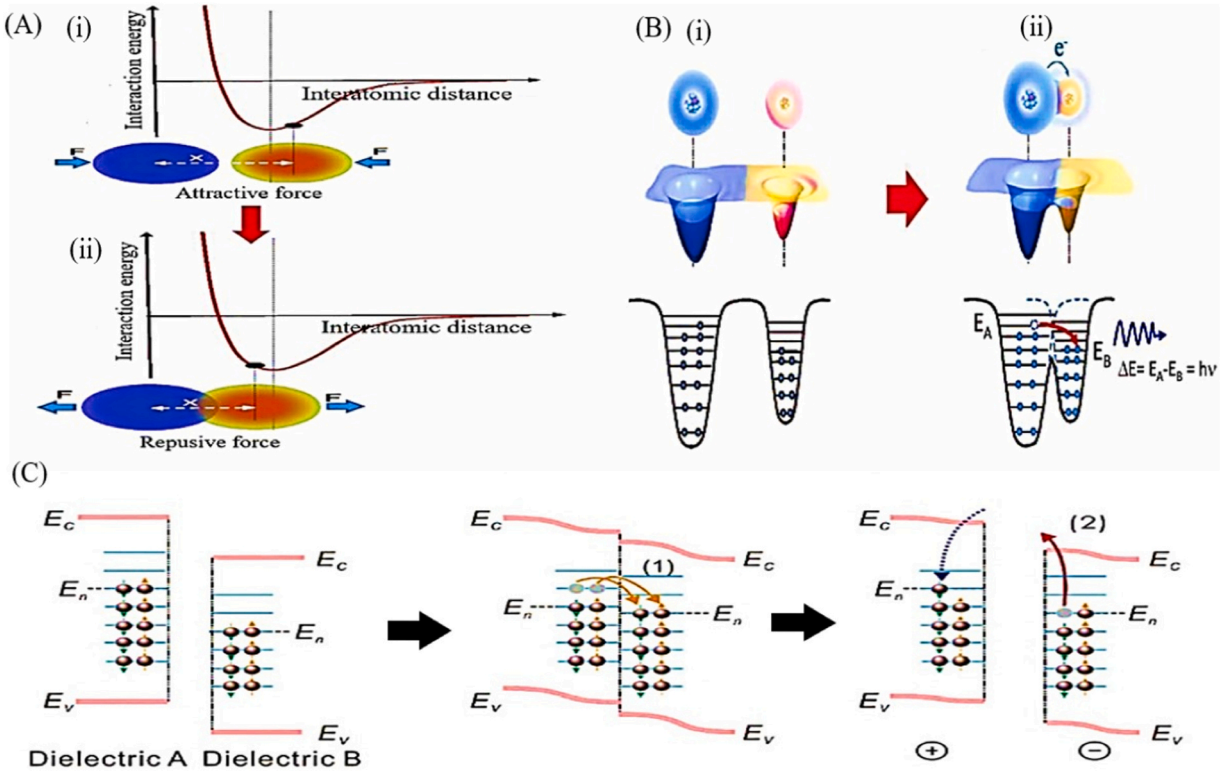

Fig. 1. Schematic of electron cloud model describing contact electrification (CE) and charge transmission between two atoms. (A) (i)(ii) Interatomic interaction under compressive force (attractive and repulsive condition).(B)(i)(ii) Illustration of the electron cloud and potential energy well model for two different conditions that are separated and in close contact, respectively. The low potential barrier between material pairs makes it possible to transition to CE.(C) Surface state model with charge transmission: prior interaction, during an interaction, and after contact between two unlike dielectric materials, for instance, that electronegativity E_n of the 1st dielectric is greater than that of the2nd. [42] (A) Reproduced with permission [2]. Copyright 2020, Wiley-VCH. (B) Reproduced with permission [2]. Copyright 2020, Wiley-VCH. (C) Reproduced with permission [42]. Copyright 2019, Elsevier.

applied, creating a minimum atomic distance of X. An intrinsic pressure arises at the minimum interatomic distance that causes a significant electron transfer. Electron transfer occurs in the repulsive force condition only, which refers to a strong overlap of electron cloud or wave function shown in Fig. 1B(i-ii) [2]. The surface state model shows the electron transfer between two dielectrics that are shown in Fig. 1C [43]. The surface and probable point defects occur due to the surface and defect states in the band gap, i.e. the conduction and valence bands [44]. Since the unoccupied surface state of dielectric A is lower than that of dielectric B, upon contact negative charge transmission occurs from dielectric A to dielectric B (Fig. 1C). Fundamental physics describe the TENG principle which is originated from Maxwell's displacement which is [41,45] defined as,

$$J_D = \frac{\delta D}{\delta t} + \frac{\delta Px}{\delta t} = \varepsilon \frac{\delta E}{\delta t} + \frac{\delta Px}{\delta t} \quad (1)$$

Where D refers to the electric displacement field and J_D is the total displacement current density, Px denotes polarization field, which is generated by electrostatic surface charges due to triboelectric effect. E and ε refer to the electric field and vacuum permittivity, respectively. The term ε (δE/δt) indicates that induced current originated through the varying electric field, which is responsible for electromagnetic waves in TENG. Another term for Eq. (1) that is δPx/δt refers to the current point to surface polarization that gives birth to the nanogenerators. The surface integral of total displacement current J_D is the required displacement current (I_D) and is written as

$$I_D = \int J_D \, ds = \int \frac{\delta D}{\delta t} \quad ds = \frac{\delta}{\delta t} \int \nabla . D \quad dr = \frac{\delta}{\delta t} \int \rho \quad dr = \frac{\delta Q}{\delta t} \quad (2)$$

Where Q and ρ denote total free charges and distribution of charges in space, respectively. Eq. (2) shows that displacement current is dominant in the internal circuit of TENG, whereas capacitive conduction current is in the external circuit.

Working mechanism of biomechanical motion driven of TENG

Biomechanical motion-driven triboelectric nanogenerator can produce voltage from random ambient body movement (e.g. distant running, walking, cardiac compression, exhale and inhale during breathing, etc.). Biomechanical energy harvesters are frequently used in wearable sensors and implantable devices. Fig. 2A(i-ii) shows an implantable magnet triboelectric nanogenerator (m-TENG) in which polytetrafluoroethylene (PTFE) and titanium were used as friction layers, magnetron sputtered Cu film as an electrode and PDMS film used as encapsulation layers [40]. A pair of the magnet was put on the back of two layers and its' repulsion force was used as a spacer (Fig. 2A(iii)). The energy harvesting principle is shown in Fig. 2A(iv). When m-TENG was implanted subcutaneously in streaky pork, biological movements create periodic loading and unloading that resulted in opposite charges depending on the polarity of materials. A compressive force causes a strong contact between two surfaces. During unloading force, two layers separated due to repulsion of magnetic force thus generating a potential drop in one material and rise in another. The free charges then drive from one electrode to another via load to compensate for voltage drop and produce a half cycle of AC. Then further application of force generates a reverse flow of electrons to complete the full cycle. The output voltage in the open circuit condition was 70 V and in short circuit current, the transferred charge was 0.55 μA, and 25 nC respectively irrespective of its encapsulation and implantation under subcutaneous tissue (Fig. 2A(v)). Thus biomechanical energy can be harvested from body movement. The abovementioned

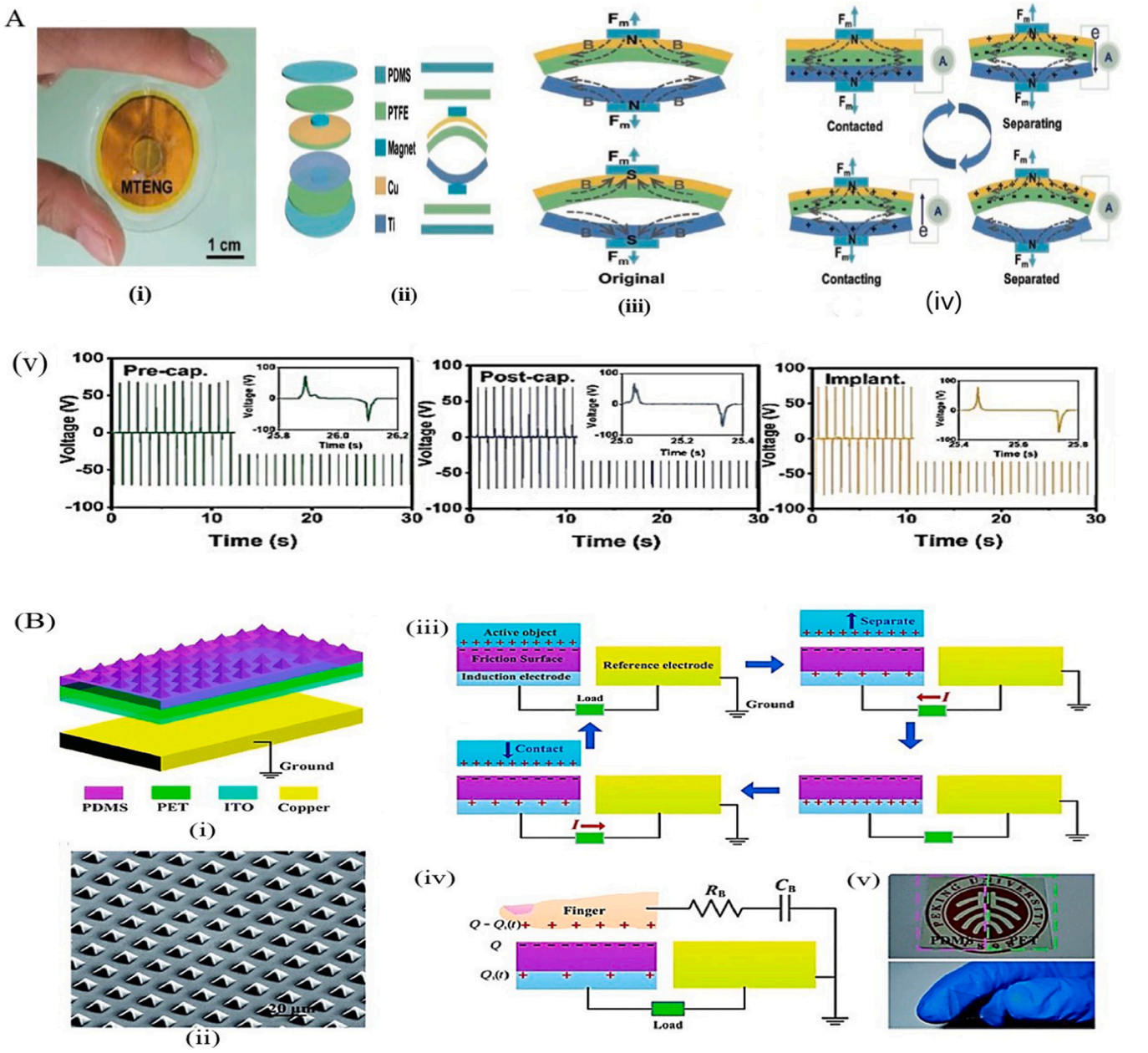

Fig. 2. (A) Schematic illustration of (i) device structure of encapsulated 3D m-TENG. ii) friction layers and electrodes of m-TENG. iii) neutral state condition. The two friction layers separate from each other due to magnetic repulsion. iv) Working principle of the m-TENG. v) V_{oc} graph of the m-TENG before encapsulation, after encapsulation, and implanted subcutaneously in streaky pork. (B) Energy harvesting mechanism of the S-TENG i) Schematic of the single friction surface TENG (S-TENG) ii) The micro-structured PDMS triboelectric friction surface iii) the triboelectric friction surface shows a tendency to attract electrons since in contact with the active object iv) equivalent circuit model of the S-TENG upon stimulation by a human finger. v) Photo of the S-TENG demonstrating high transparency and flexibility.
(A) Reproduced with permission [40]. Copyright 2019, Wiley-VCH. (B) Reproduced with permission [47]. Copyright 2015, Wiley-VCH.

biomechanical motion TENG harvest biomechanical energy using two electrodes that are attached to moving layers of TENG. However, the deposited electrode attachment causes difficulty in real-time application in biomechanical energy harvesting. To address the issue single electrode-based TENG is introduced in which one electrode and layer interact with the object only and the other electrode serves as a reference electrode that provides electrons [47]. Micro-patterned PDMS triboelectric layers were deposited onto both the ITO electrodes and PET substrates (Fig. 2C (i-ii)). Copper electrodes serve as reference electrodes and are connected to the ground. The working mechanism is shown in Fig. 2C(iii-iv). When an object touches the PDMS layer, it produces charges at the interface. After the separation of the object from the PDMS surface, the free-electron drive to the ITO electrode. These charges balance the electrostatic field distribution in the ITO electrode that was created by the triboelectric charges remaining on the PDMS layer and result in generating a currents pulse. Again the second contact on the PDMS layer compensates the triboelectric charges and the free charges amassed in the electrode move back into the circuit to generate a second current pulse opposite to the first one. Thus electrical energy can be harvested simply from any object coming in contact with the triboelectric layer of PDMS. A prototype (Fig. 2C(v)) showed that tapping with a polyethylene (PE) glove rather bare hand can produce 40% more voltage and replacement of the PDMS layer with PET substrate reduce the performance by 30%. However, this mechanism paved the way to harvest biomechanical energy from the promising skin surface.

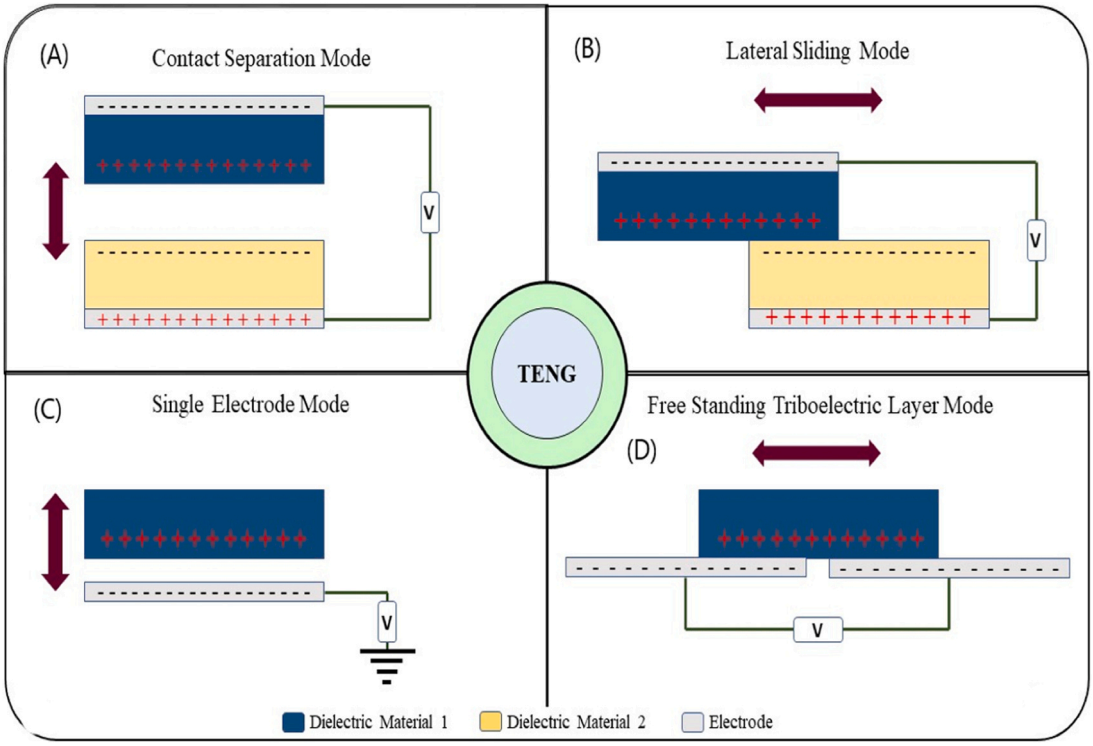

Fig. 3. Illustration of four basic modes for TENG operation: (A) vertical contact mode, (B) lateral sliding mode, (C) single electrode mode, and (D) free-standing triboelectric layer mode.
(D) Inspired from [47]. Copyright 2015, Wiley-VCH.

TENG operation modes

Triboelectric nano-generator uses four basic modes of operation based on the motion of the layers and electrode arrangement [46,47] known as contact separation (CS) mode, lateral sliding (LS) mode, single electrode (SE) mode, and free-standing triboelectric (FT) layer mode to generate alternating current (Fig. 3(A-D)). Triboelectric surface charge density, surface structure, dielectric properties, and material robustness are the key factors contributing mostly to TENGs performance [48–50]. Zhu et al. [51] described the CS mode where electricity conversation uses contact electrification and electrostatic induction. The author used poly-methyl methacrylate (PMMA) and polyimide (KAPTON) as desired materials and describe a complete sequence of electricity production procedures in open and short circuit conditions of CS mode. Electricity generation uses contact and separation of two dielectric layers under periodic loading and unloading. CS mode is found feasible to collect energy from the shoe insole and cardiac rhythm of the body to power drug delivery devices or pacemakers.

LS model uses a similar principle of periodic contact and separation between two dielectric layers of different materials [52,53]. Triboelectric energy is generated from the friction force when the lateral sliding movement of parallel surfaces occurs. The relative displacement of two planes and corresponding potential generation in LS mode provides more benefits than in CS mode since power conversion efficiency increased enormously because of full layers of contact [47]. Because of increased contact and friction force, there is a high level of erosion between materials, which leads to a low life expectancy. However, PTFE nanoparticles [54] or macro balls and macro rods provide [55] satisfactory results to successfully address this problem. Some research showed that lateral sensitivity, cycle speed, and contact-separation process in every cycle could be increased significantly or even multiple times using a simple grated structure [54,56,57]. Joint movements of humans are the main sources to generate energy using LS mode. Ankle joint and elbow joints based TENG was already implemented in the TDD system that uses LS mode operation [58].

Arbitrary and free movement energy harvesting is frequently hindered by double electrode design, i.e., CS and LS modes. Such a close circuit double electrode scheme limits the practical application of TENG's energy collecting that must be attained. SE mode was introduced to address the issue of the double electrode close circuit strategy [59] and extensive research was performed in 2014 [60–63]. SE mode uses periodic contact-separation of the moveable layer and its electrode with the moving body while other electrodes serve as a reference electrode (e.g., conductor or grounding) that is the continuous source of electron supply. Both the CS mode and LS mode can be implemented in SE mode and used in TENG-based TDD [64].

FT layer mode uses two electrodes underneath a moving layer separated by a gap. The moving layer is charged using triboelectrification before moving on the electrode. Electrically charged moving layers generate an asymmetric charge distribution and subsequent electron flow while moving between the electrodes. FT layer mode has some advantages like high energy conversion and robustness [65] rather than other traditional mode operations. Its versatility and easy adaptability provide some extra benefits for arbitrary movement energy harvesting from human locomotion or gait cycle without an attached electrode similar to SE mode. Triboelectric series (developed by Alpha Lab) used as a reference for TENG development [66,67] and figure of merits used to compare common standards among TENGs [68].

Transdermal drug delivery principle

TDD provides an interesting alternative to oral drug delivery and is poised to represent an alternative to hypodermic injection [69–72]. TDD expands its application from pharmaceuticals to skin care industries because of its low rejection rate, convenience and

persistency among patients, and superb ease of administration. TDD ensures the prevention of nonspecific delivery to cells and tissues that are not targeted by the drug and also inhibits local buildup in drug concentration [73]. The major challenge in TDD is the paucity of drugs that are amenable to administration by this route. It is difficult to use transdermal routes to deliver hydrophilic drugs, peptides, and macromolecules (e.g. DNA, small interfering RNA) that possess particular challenges [74]. To address this issue, electrical stimuli-based delivery has been introduced to deliver drugs and extract molecules (analytes) through the skin [75]. TENG-based drug delivery use iontophoresis, sonophoresis, and electrophoresis principles to deliver drugs with optimum accuracy and control.

Iontophoresis

Iontophoresis enhances TDD with accurate control by applying continuous low voltage current to the skin. Iontophoresis allows TDD through the ions manipulation, which occurs due to electroosmosis and electromigration [4]. The main benefit of iontophoresis is that the drug delivery rate can be achieved with precise controllability of the parameters and electrified time [76]. Iontophoresis-based TDD has already been performed and its commercializing process is on its way. Gelfuso et al. [77] examine iontophoresis for voriconazole delivery that showed the capability of iontophoresis to increase drug penetration and potency. In addition, it was found that a precise amount of ropinirole hydrochloride could be delivered through the skin in different current densities, which permitted the customized treatment of Parkinson's disease [78]. Despite being an excellent technique for the delivery of small drugs (e.g. diclofenac, calcein [79,80], and methotrexate [81]), iontophoresis showed limitations for macromolecules (e.g. proteins) due to the stratum corneum [82,83]. Although iontophoresis provides numerous benefits in the TDD system, its application is often hindered by the need for a bulky power source. To overcome this issue microneedles iontophoretic method has been used extensively, which has shown synergistic effects, increase flux and enhancing skin permeability [84,85]. Yang et al. [86] proposed an iontophoresis-microneedle array patch (IMAP) to deliver macromolecular drugs. Insulin was encapsulated in positively charged nanovesicles to improve drug permeation due to electrostatic interactions and electroosmosis. The IMAP combined with iontophoresis and nanovesicles showed safe and synergistic enhancement of the in vivo treatment of type 1 diabetes. Results showed excellent control over body glucose level and sufficient avoidance of hypoglycemia with the highest normoglycemic state for 6.8 h which was 3.1 times higher than the injection group. Fig. 4 shows a schematic diagram of the iontophoresis principle in which repulsion of drug cations are moved through the skin due to electro-repulsion [87]. A bunch of molecules with physicochemical properties like molecular weight <500 Da, low melting point, and adequate lipophilicity are able to penetrate the skin only due to the stratum corneum. However, iontophoresis assists to overcome the strong barrier properties of the stratum corneum using small current pulse to skin. Smartphone powered the iontophoresis driven circuit, that stabilizes input voltage and outputs current. The TENG-based power source could be a feasible way to attain this inconvenience and exploit this promising method in drug delivery. TENG power TDD system employing iontophoresis was first reported in 2019 [35] and extensive research is going on for its commercialization. This integrated system seems very promising for future transdermal drug delivery.

Sonophoresis

Sonophoresis (SP) provides a microstreaming flow of ultrasound to the proximity of skin that helps augmentation of shear stress to the stratum corneum and results in channels for transdermal drug delivery [88]. It was reported that ultrasound provokes thermal effects on the sonophoresis skin that positively influence skin permeability coefficient and drug diffusion coefficient [89]. However, the intensity of SP is not sufficient enough to impact the molecular kinetic energy of the influenced tissue and drugs substantially. Moreover, thermal energy sometimes causes heating damage to the thermally unstable drugs [89]. To overcome these inconsistencies, SP combined with iontophoresis to minimize thermal effects. TENG has an immense opportunity to replace bulky power sources used in SP and provide small sizes, portable, and cost-effective compelling solutions in this case. SP found it handy for insulin delivery because of its long-term treatment of diabetes, cost, and inconveniences in the syringe. Feiszthuber et al. [90] investigated transdermal insulin transport into skin agar model and porcine skin in vitro using SP. Results showed a remarkable increase in insulin delivery for both models, but the agar model showed much penetration depth with satisfactory output. In another work, Yu et al. [91] compared commercial transdermal patches with sonophoretic delivery of rivastigmine (RIV) on porcine skin using a 20 kHz ultrasound frequency. Results showed that RIV permeation enhances remarkably by low-frequency sonophoresis on the back skin of suckling pigs. The in vitro study indicated that the steady-state transdermal flux and excised skin permeation after 24 h of sonophoresis increased significantly by a factor of 3.1 and 2.99 times respectively, compared to control groups (Fig. 5A. (i)). The plasma concentration vs time graph is shown in Fig. 5A(ii) after the administration of RIV containing the coupling medium (gel-like liquid used between skin and transducer probe). The maximum concentration was found 0.83 ± 0.16 and 0.28 ± 0.07 $\mu g mL^{-1}$ for the sonophoresis and the control group, respectively. Acoustic cavitation was considered the key mechanism of action in sonophoresis-mediated enhancement in TDD. Pharmacokinetic parameters (e.g. drug concentration in blood) were measured using the HPLC-UV method which showed a satisfactory result in this study. Furthermore, Bok et al. [92] combine both sonophoresis and iontophoresis techniques to deliver hyaluronic acid (HA) and rhodamine B in vitro using gelatin hydrogel (Fig. 5B). It was found that permeability of the material serves as a key factor for the material property. This study showed that combining both iontophoresis and ultrasonication in microneedles enhances permeation, thus reducing the delivery time required for the passive or ultrasonication alone. The result highlights the significance of the combined principle in drug delivery. The author anticipates that this system could be feasible for macromolecular and dependence delivery in the future based on drug response time.

Electroporation

Electroporation requires high voltage pulses of electricity to create aqueous pores that are essential for percutaneous transport. Electroporation serves as an important method of TDD and is being investigated for its synergistic effects with sonophoresis. EP-based skin permeability is contingent upon some specific characteristics of electrical pulses that as time duration, pulse shape and number, and amplitude of the pulses. Among these properties, pulse length and amplitude play a crucial role in electrical attributes, and finding the balance among parameters is the main challenge in EP research [93]. Liu et al. [94] developed a nanoneedle electroporation-based intracellular drug delivery that ensures high efficiency, on-demand delivery, and minimal cell damage (Fig. 6). A hand-powered TENG was used to generate an electric pulse between cathode and anode. For the in vitro study, TENG-generated electric pulses pass through the nano-needles and cause electroporation in the cells (Fig. 6A). The in vivo delivery is shown in Fig. 6B in which a rectangular free-standing TENG was used to cause electroporation. Nano needle electrode serves as an anode and is attached to the mice's skin whereas a stainless-steel needle was embedded under dorsal skin as

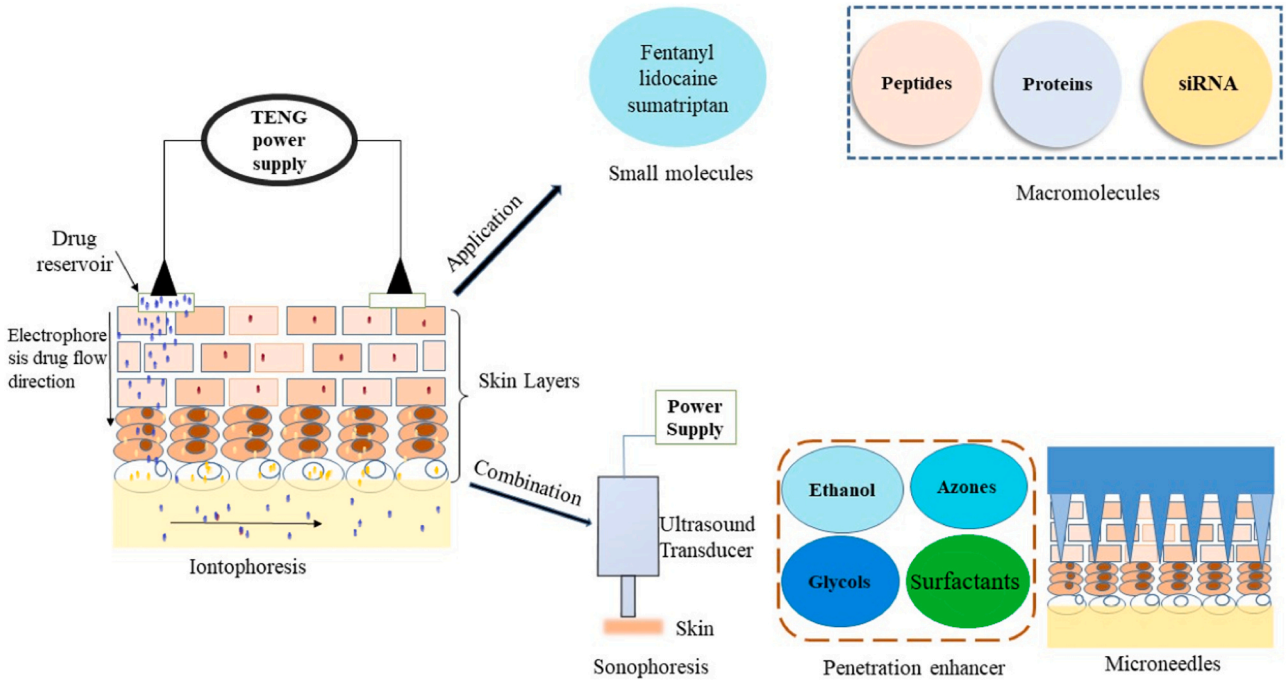

Fig. 4. Schematic of TDD system using iontophoresis principle. The combination of multiple drug delivery principles and influencing factors enhance the flow rates of micro molecules and macromolecular drugs.
Reproduced with permission [87]. Copyright 2021, Springer Publishing Company.

a cathode. To minimize cell damage [95–97], the author chose a single electrode with a pointed tip (Fig. 6C). An electric field simulation showed an applied voltage of 20 V and the increasing electric field confined at the peak of each needle up to ~2800 V cm^{-1}. (Fig. 6D). The result showed that this integrated system was able to deliver small molecules, siRNA, and macromolecules with a delivery efficiency of 90% and cell viability of 94%. EP-based micro/nano needles serve as another promising approach in transdermal drug

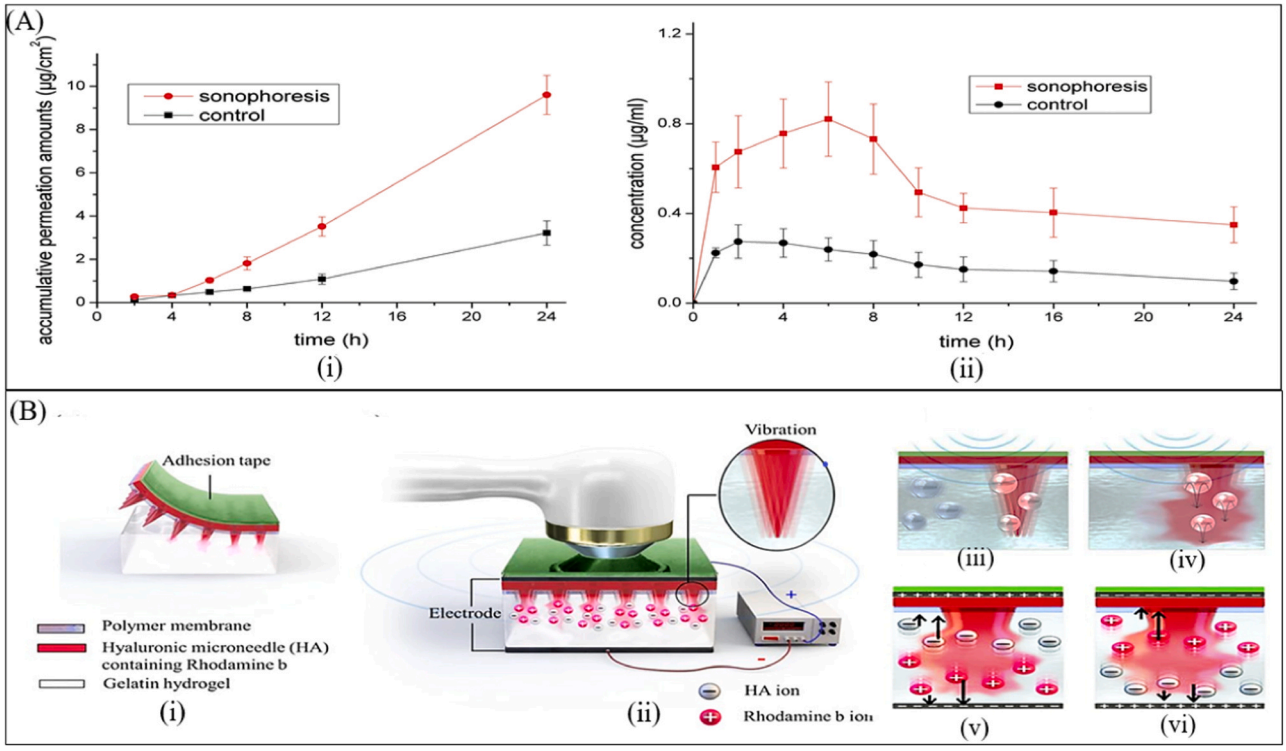

Fig. 5. Schematic of sonophoresis TDD principle. (A) (i) penetration of RIV through excised pig skin and plasma concentration-time graph. (ii) administration of RIV containing couple media. (B)(i) Hyaluronic microneedle (HA) attachment in gelatin hydrogel. (ii) Combination of electric field and ultrasonic vibration in gelatin hydrogel. The inset image shows the vibration in the HA microneedle. (iii) Dissolution of HA microneedle upon vibration. (iv) The prediction dissolution mechanism and ions flow direction under the effect of electricity. When (v) voltage > 0 (vi) voltage < 0.
(A) Reproduced with permission [91]. Copyright 2015, Avoxa-Mediengruppe Deutscher-Apotheker GmbH. (B) Reproduced with permission [92]. Copyright 2020, Springer Nature.

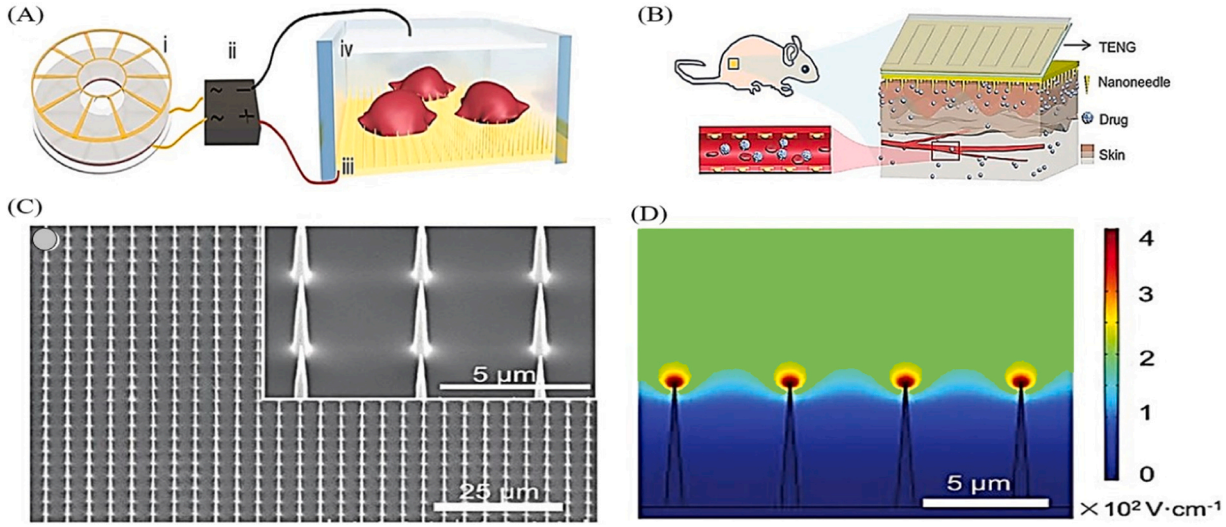

Fig. 6. Schematic illustration of TENG driven in vivo electroporation system. (A) the in vitro electroporation system (B) the in vivo electroporation system (C) Scanning electron microscopic image of the silicon nano-needle array (D) Electrical field distribution of the nano-needle array under a 20 V electrical potential.
(D) Reproduced with permission [94]. Copyright 2019, Wiley-VCH.

delivery that takes advantage of both transdermal patches and hypodermic syringes [98]. The microneedle system provides some advantages: i) site-specific delivery with exact penetration depth ii) painless drug delivery with a high flow rate of drug iii) minimal skin damage with the flexibility of uses at any time. To ensure a high output delivery Pamornpathomkul et al. [99] tested the combined effects of low-frequency SP with microneedles in vitro TDD of fluorescein isothiocyanate dextrans (FSD). The result showed the greatest delivery at combined technique rather than individual method. In addition, Tokumoto et al. [100] examined IP with SP or EP to evaluate their impacts on electro-osmosis. The electroosmotic activity of mannitol into mouse skin showed substantial enhancement for SP with IP, while EP demonstrated no notable changes to mannitol flux. Conversely, a comparative study of each possible combination: EP, microneedles, and SP by Petchsangsai et al. [101] for percutaneous delivery of FSD showed incorporation of all these methods performed synergistically to enhance skin permeability. The highest amount of FSD transport that is 16.58 ± 2.35 μg/cm^2/h was recorded and permeability was found 100 times greater than that of individual SP. Comprehensive study among these method suggested that combination of any two or three might be handy for each aspects of TDD.

High-performance TENG structure for drug delivery

Because of the low side effects and non-invasive manner, TDD retains more benefits than usual drug delivery means like oral or injection [102]. TDD is considered promising for several benefits like (i) it successfully bypasses the first-pass effect of both gastrointestinal and hepatic (ii) ensures stable and durable blood concentration (iii) convenient to use and termination at any time (iv) improvement in patient compliance. Electrically stimulated drug carriers are used to deliver the drug to a specific site in a precise way. Ouyang et al. [35] proposed an iontophoresis patched-based TENG structure to deliver the drug. The TDD system consisted of three components: TENG, power management unit (PMU), and patches (drug patch and iontophoresis patch) (Fig. 7A(i)). The drug-loaded electrode and counter electrode are unified in screen-printed electrodes (SPE) (Fig. 7A(ii)). Upon electrical stimulation, PPy film releases the drug from the drug patch. Active drug transportation is needed for effective and deep penetration in the skin that is achieved by iontophoresis by controlling a bidirectional switch in a circuit. The author used dexamethasone sodium phosphate (DEX-P), which is frequently used in inflammation and allergic reactions to musculoskeletal injuries [103]. Using electro-polymerization, the author electrodeposited the DEX-P-loaded PPy spongy layers onto the electrode. Anionic charge DEX-P is loaded into the polymer matrix of the pyrrole to balance positive charges on the backbone surface of PPy films. High drug loading capacity and increasing surface area of the PPy films were gained by using nanostructured pores in the PPy films. When an electrical stimulus (negative voltage ~ −0.8 V to ~ −1.5 V) is given to the PPy films via electrodes, it is electrochemically reduced and releases DEX-P into the skin surface and subsequent neutralization occurs in PPy backbone surface [104,105]. Iontophoresis treatment was given using a patch electrode (Fig. 7A(i)). After the application of voltage using electrodes drug molecules penetrates the skin due to electrophoresis and electro-osmosis. The drug release rate was calculated for every 20 min of electric stimulus with a pause of 60 min and a comparison was made between conventional power delivery devices and TENG. The drug release amounts in a 60-minute time duration were 35 μg/cm^2 and 27 μg/cm^2 for TENG and potentiostat, respectively. This radial array TENG (Fig. 7A(iii)) increases the drug delivery rate significantly and the most notable feature of this delivery system was the tunable delivery that can tune the delivery rate from 0.05 μg/cm^2 to 0.25 μg/cm^2 per minute by altering TENG charging time or resistance in PMU. Despite achieving a promising result, this rotatory structure TENG is not suitable for energy harvesting from regular human movement. Flexible design and size reduction could be a feasible way. However, size reduction has a crucial impact on TENG output and power supply to the drug-loaded patch which could reduce the operational accuracy.

In another work, Wu et al., [58] suggested a CS mode-based insole TENG to deliver cationic drug (e.g. Rhodamine 6 G (R6G) & methylene blue (MB)) in which the drug patch was made using two side by side hydrogel cells embedded with carbon cloth electrode (Fig. 7B(i)). Between these two cells, one cell was preloaded with R6G during fabrication. R6G is a fluorescent organic dye used as a contrast medium and MB is used to treat urinary tract infection, methemoglobinemia, and cyanide poisoning for medical purposes. The TENG used polytetrafluoroethylene (PTFE) as triboelectric material and aluminum (Al) as other triboelectric material and electrode, polyethylene terephthalate (PET) as substrate, and Kapton as a spacer. This TENG was able to produce an open circuit voltage of

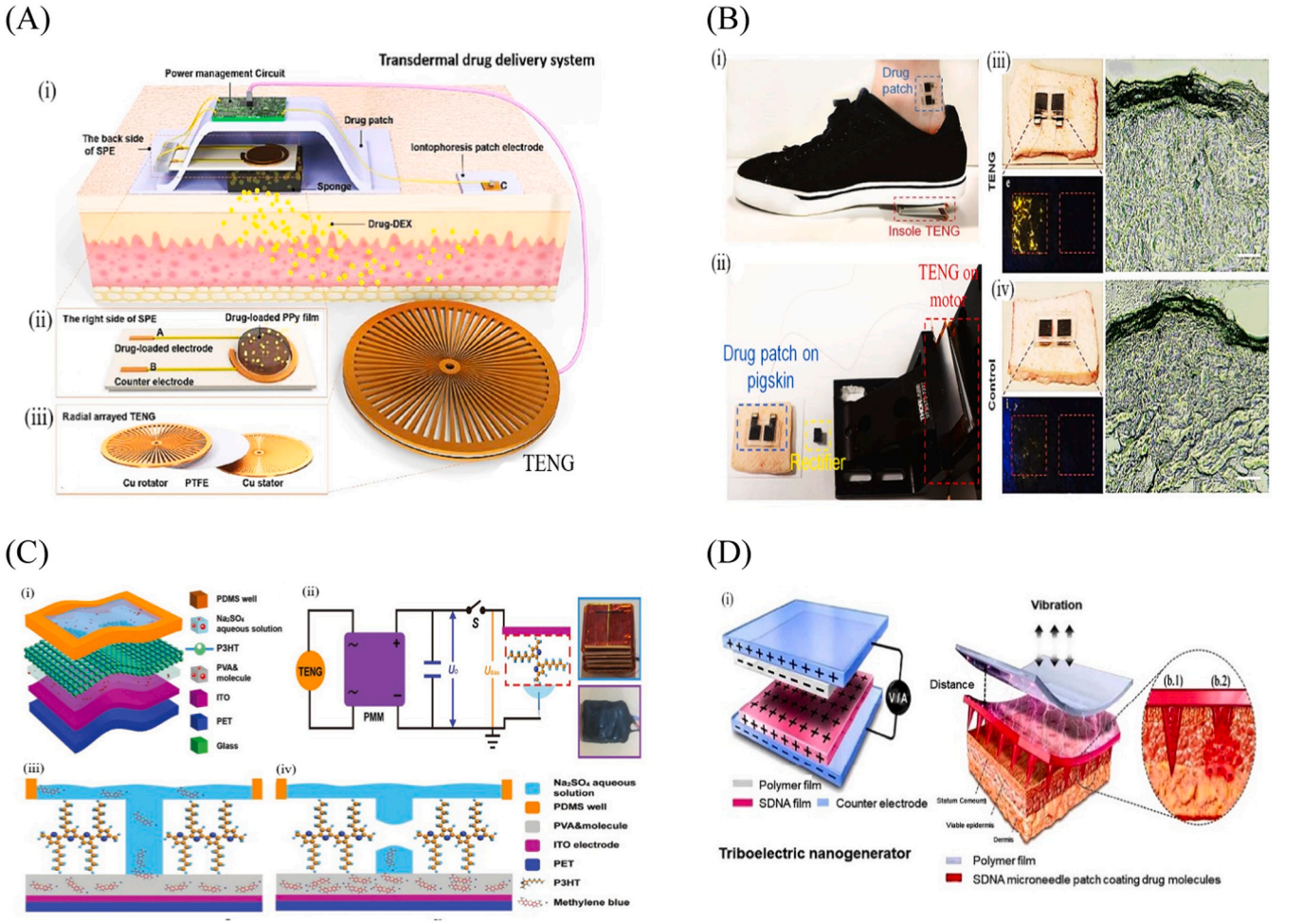

(caption on next page)

Fig. 7. Schematic representation of the self-powered TDD system. (A) (i) parts of the system ii) right side view of the SPE (iii) dielectric material layers of radial arrayed revolving TENG. (B) (i)Photographic illustration of wearable TDD system: insole TENG, designed drug patch (ii) full experimental setup with foot motion simulated by a linear motor (iii) R6G containing hydrogel drug patch on pig skin connect with TENG. The bright field cross-sectional histological images (bottom) and fluorescent cross-section histological images (right). (iv) R6G containing hydrogel drug patch on pig skin connect without TENG. The bright field cross-sectional histological images (bottom) and fluorescent cross-section histological images (right). (C) Schematic illustration of the FDRD (i) parts of the FDRD: PET substrate film (60 μm), ITO electrode, PDMS well, PVA/P3HT functional multilayers (ii) circuit schematic of self-powered releaser; inset figure(top) is a TENG, and a PMU (bottom) (iii) The micro molecule released from (polyvinyl alcohol) PVA layer to the sodium sulphate aqueous solution after the switch turn on, (iv) following the switch turn off, penetration of molecule through P3HT film stopped. (D) (i) SDNA-based TENG physical structure. Coupling of drugs loaded SDNA microneedle and vertical vibration-based triboelectricity in the porcine cadaver skin, (b.1) magnification of the microneedle insertion area, (b.2) microneedle dissolution in the porcine cadaver skin. (E) Illustration of implantable magnetic TENG-driven drug delivery in vivo. (i) Infographic illustration shows the DOX loading into red blood cells and its release under the control of implantable TENG (ii) Micro-imaging of DOX loaded RBCs in tumor site of nude mice. In vivo imaging provides blood circulation and amassing of the D@RBCs to tumor sites at 6, 12, 24, 48, 72 and 96 h respectively. Illustration of Ki67 immunohistochemistry pictures of the tumors in different groups (measuring bar: 200 μm). (iii) Image of the collected tumors in different sets after one month of investigation. Reproduced with permission [111]. Copyright 2019, John Wiley & Sons, Inc.
(A) Reproduced with permission [35]. Copyright 2019, Elsevier. (B) Reproduced with permission [58]. Copyright 2019, John Wiley & Sons, Inc. (C) Reproduced with permission from [3]. Copyright 2020, John Wiley & Sons, Inc. (D) Reproduced with permission [29]. Copyright 2018, The Royal Society of Chemistry. (E) Reproduced with permission [111]. Copyright 2019, John Wiley & Sons, Inc.

1200 V with a short circuit charge transfer of 370 nC per cycle and an optimum short circuit current of 20 μA. To assess the performance of the TENG-driven iontophoretic TDD system, pig skin was taken as a surrogate for human skin. Since the R6G was cationic, the electrode on the drug-loaded hydrogel patch was connected to the positive side of the rectifier to the TENG and the other electrode to the negative end. The linear motor was used to operate the insole TENG, and drug patches were placed in an oven (at 37°C) to simulate body temperature (Fig. 7B(ii)). The result showed that approximately 320 nC charge was delivered per cycle and an 8 V AC peak to peak voltage was achieved. After rectification, the pulse DC and voltage reached 12 μA and 4 V, respectively. TENG stimulates the ion inside the hydrogel drug patch and since the drug patches were separated by a polydimethylsiloxane (PDMS) frame, the easiest route for the drug was to drive through the skin. Thus, the model drug penetrated through the skin because of electricity, and TDD was achieved via iontophoresis. To compare the result a control experiment was accomplished by the author without any TENG connection to the patch. Results showed that under a 365 nm UV lamp, fluorescent images from TENG operating device depicted strong delivery of R6G compared to the control group (Fig. 7B(iii-iv)). This TDD provided a cost-effective solution without complex components and advanced modular design enabled the reuse of components with different drug patches. Therefore, the proposed work provides a noninvasive and electrically assisted TDD solution with closed-loop sensing and treatment which was promising in biomedical treatment.

Furthermore, Liu et al., [3] proposed TENG powered flexible drug release device (FDRD) using the surface wettability-based switching to release methylene blue, R6G, and fluorescein sodium like small molecules (Fig. 7C(i)). Electro-wetting manipulates liquid's wettability on a dielectric solid which is essential for controlling fluids velocity in a micro-channel [106,107]. Hence, it controls the drug release rate precisely. The main disadvantage of this method is the high switching voltage requirement. To address this issue, the performance of the TENG was increased by employing a micro-nano-pattern on the fluorinated ethylene propylene (FEP) surface by inductively coupled plasma (ICP) etc. The CS mode-based TENG provides a steady voltage supply to release drugs and the unique switchable wettability of poly (3-hexylthiophene) (P3HT) films in sodium sulfate solutions was regulated (Fig. 7C(ii)). TENG harvest energy from body movement and provide this energy to the power management module (PMM) unit. PMM supply a steady bias voltage of 1 V to the FDRD releaser. This bias voltage oxidized the solution and changes the contact angle of the Na_2SO_4 solution from 106° to 59° sharply. After turning on the switch, a steady bias voltage creates hole in the backbone of P3HT chains and it changes from hydrophobic to hydrophilic nature thus small molecule can easily release in it (Fig. 7C(iii)). When the mechanical switch turns off, the release is stopped because of the change in surface tension in opposite surface and the transition to hydrophilic state from hydrophobic state of P3HT (Fig. 7C(iv)). With this wettability mechanism, a controlled release of wound healing drug delivery was achieved with high precision, flexibility and permeability.

In addition, Bok et al. [29] proposed another method to facilitate TDD systems using drug-loaded micro-needling arrays shown in Fig. 7D(i). It replaces the existing electrophoresis method and proves more convenient for releasing drugs. One of the TENGs dielectric layers and dissolving microneedles were made from salmon deoxyribonucleic acid (SDNA) that can provide sufficient biocompatibility and leave biohazards. To maximize drug release efficacy and output voltage of TENG, chargeable polymers (Polyimide & Teflon) were compared by the author with SDNA film. Porcine cadaver skin was used to test and analyze the mechanical performance of microneedles. Simultaneous triboelectric induction due to contact separation of layers returns electric charge that was delivered to the drug intercalated SDNA microneedles. The output voltage was found ~95 V while the voltage during drug release was larger than it, which indicates triboelectric behavior depends on the drug intercalated SDNA surface. Negatively charged protein residue inside the skin amasses negative charge on the skin surface and corresponding positive charge induction in Teflon and microneedle patches. Current flow occurs due to the reduction of internal body resistance. Approximately 0.1 MPa load can produce ~80 V output voltage in Polyimide-SDNA and ~100 V output voltage in Teflon-SDNA film, respectively. It was found that output voltage is contingent upon applied forces besides surface contact. A change of force from 0.1 MPa to 0.2 MPa increased 50 V potential in Teflon-SDNA films. Applicability of the microneedle device was tested for an SDNA based TENG device holding a drug molecule of hydrolyzed sodium hyaluronate (HA). The result showed a reciprocal relationship between drug concentration and output potential; an increase of HA concentration from 1% to 10% wt reduced the output peak from 150 V to 80 V. This result indicates that high drug concentration in SDNA film reduces output voltage. Output current follows the same pattern of decreasing that is 70 μA to 20 μA. Bovine skin is a derivative of gelatin hydrogel used as model tissue and rhodamine dye inside microneedle to form a colorized image to omit the opacity and retain actual skin behavior. Rhodamine emissions increased after 15 s every time and increased from 50 ng (only microneedle attachment) to 220 ng (at triboelectrification) within the 60 s. Thus, TENG-driven drug delivery provides excellent results for manageable drug release both in vivo and in vitro.

Doxorubicin (DOX), a regularly used chemotherapeutic drug for killing carcinomatous cells, i.e. solid and hematopoietic tumor cells [108–110], still have side effects: cardiotoxicity, alopecia, myelosuppression, and mucositis. Targeted drug delivery provides the possible solution for these shortcomings and improves drug efficacy by increasing controllable drug release to the auspicious site. Zhao et al. [111] reported DOX-loaded red blood cells (RBCs) in tumor DDS using implantable magnetic TENG, which showed astonishing results in both in vivo and in vitro studies (Fig. 7E(i)). DOX was loaded in RBCs (D@RBCs) using a hypotonic dialysis method that mixes

pristine RBC suspension and DOX with 200 μg mL^{-1} concentration. In vivo investigation of HeLa-malignant tumor-bearing BALB/c-nu mice is shown in Fig. 7E(ii). m-TENG produced an electric field (EF) that was supplied to the tumor site using steel microneedle electrodes. Results showed that applied EF boosted drug release by creating nanopores on RBCs surface and auto-healing of pores after EF drowned. D@RBCs were injected into nude mice and their distribution at different periods was monitored using an in vivo imaging system. Maximum D@RBCs amass at the liver site after 6 h of inoculation and remain till 24 h. At 48 h its distribution in the liver is approximately identical to the tumor-bearing site. DOX signal at 72 h after vaccination showed a great variance for both the tumor and liver site, while the liver exhibited significant declination but tumor slight. The study was conducted on 60 nude mice, classified into six groups treated with D@RBCs, PBS, DOX, EF, DOX+EF, and D@RBCs+EF. The EF and PBS group shows uncontrolled and rapid differentiation of tumor cells i.e., tumor volume increased. DOX effect provides a reasonable growth inhibition that indicates that simple chemotherapy was unable to decimate the tumor. DOX+EF groups are juxtaposed with the DOX-only group while comparing their function. A momentous reduction in tumor growth was found in the D@RBCs group; assumed accumulation of D@RBCs in the tumor due to the EPR effect. The best output was found from D@RBCs+EF; a combination of drug and TENG stimulation. After 30 days of treatment, half mice were executed and tumors were collected from each group shown in Fig. 7E(iii). The D@RBCs+EF demonstrate minimum tumor volume with huge growth suppression. Ki67 immunohistochemistry images, refer to a reduction of tumor cell propagation in the D@RBCs+EF group (Fig. 7E(ii)) bottom image. The body weight of the surviving mice remained the same which indicates a positive sign with no harmful effects. This innocuous result and high adaptability ensure an exciting efficiency of the D@RBCs+EF group in vivo conditions.

TENG-based TDD highly depends on its output power supply. Most of the TENG implemented in TDD were synthetic polymer-based TENG. High efficiency and excellent output performance TENG are fabricated easily using infusible and insoluble biomass materials (e.g. lignin, chitosan, or cellulose) that escalate its application from miniaturized [112–114] to implantable devices [115–118]. Surface properties modification of poly-saccharide could carry out similar triboelectric charge densities in TENG layers that were previously occupied by synthetic polymers. So the necessity of biodegradable and eco-friendly TENG is unavoidable. Table 1 shows some infusible and insoluble biomass materials based on TENG and its output parameters that could be used extensively in the TDD system in the future.

Discussion

The SE mode operation-based TENG was first introduced in 2015 in microneedle drug delivery which was able to produce 26–28 V upon the friction of PDMS and Cu [162]. Within a year, TENG output reaches up to 3000 V using the CS and FT mode operation [162]. Due to its flexibility, miniaturization capability, and protean materials availability, TENG development and the growing trend in implantable and wearable sensor devices are expanding rapidly in recent years. It is hypothesized that the TENG-based power harvesting system will replace the bulky power source like batteries within a few decades. Sustainable commercialized production of TENG-based systems will expand. By combining nanocarriers, micro/nanoneedle patches, trigger-able polymer, and microfluidic devices, TENGs will provide intelligent drug delivery without the need for external energy. This self-powered delivery system has already been implemented for macromolecular delivery (e.g. protein, insulin, siRNA, DNA, etc.) and micro molecule drugs (DOX, DEX-P, FLU, SF, etc.). Despite this progression, some challenges are still encountered in its advancement that is stated below,

Challenges in perspective of epidermal drug delivery

First of all**,** materials selection for TENG devices is the most challenging task for today's scientists. Some flexible materials like KAPTON, PTFE, PDMS, and Cu/Al can generate output above 100 V [162]. But, their flexibility is restricted by the use of an acrylic sheet that is used as a supporting layer in TENG. This impedes the wearability and implantability of TENG in drug delivery devices. Biomechanical energy harvesting seems challenging because of complex organ structures and the scarcity of flexible TENG materials to design intricate structures with integrated devices. Secondly, the charge affinity of materials is firmly coupled with the materials' chemical structure, and surface charge density is quadratically proportional to TENGs' electrical output. Most of the biomechanical motion-driven TENG uses a spacer/keel structure which shows less tendency to detach and erode over time. This gives rise to a decreasing output from body movements. Although surface modification and surface functionalization enhance TENG output significantly by increasing charge affinity, continuous friction of layers result in low durability and decreasing output in TENG. Much more study is needed in nanoscale surface modification and ion injection on TENG layers to ensure long-life TENG output. Moreover, the low-pressure sensitivity and fluctuating triboelectric potential of the triboelectric layers under chemical substances like phenol, catechin acid, and heavy metal ions arrest TENG application in special environments. Robust materials and environmental encapsulation are highly needed to use TENG in multiple environmental conditions. In addition, TENG and drug delivery devices are fully independent in the aspect of electroporation, electrochemistry, and microfluidic drug delivery systems. Integration of these devices is still a challenge for present researchers to control accurate drug release. Another important issue is that the irritation occurs at the drug unloading site due to the use of iontophoresis patch hydrogels causes great concern to clinical scientists. High voltage pulse or current flow through the skin generates heat which leads to thermal cell death in many cases. Last but not least, most of the experiment is conducted on pig or mice skins that possess a slightly different skin resistance to drugs than human skin. However, the literature showed that pig skin appeared as the best possible model for human skin [163,164]. Most of the properties of porcine and human skins (e.g. lipid composition, epidermal thickness, and membrane permeability to diverse compounds) are significantly similar [165]. Despite these similarities, human trials are still at their rudimentary stage. Clinical trials in the human body must be ensured to evaluate the output performance.

Challenges in perspective of implantable drug delivery

To make TENG an implantable device for in vivo drug delivery, TENG must be more miniaturized in form with more flexibility and self-adaptability to reduce foreign body sensations and adverse effects on the human body. First of all, as an implantable device for in vivo drug delivery, TENG needed to be tiny in size with sufficient biodegradability. Biodegradable and biocompatible material-based TENG is already available at the current time. However, biodegradable TENG is limited to its output performance since it reacts faster with body components (e.g. protein, enzyme, blood pH, etc.). Hence, the attachment of TENG with biological tissues is needed further improvement to provide long-term service. It will ensure less difficulty in anchoring operations. Secondly, the power supply of implantable TENG generates thermal effects in biological tissues. Hao et al., [166] showed the effects of heat application on in vivo drug absorption from the TDD system. For some drugs, the serum peak/

Table 1
Output performance of infusible and insoluble biomass polysaccharide-based TENG.

Operation Mode	Materials	V^*_{oc} (V)	I^*_{sc} (μA)	Power Density (mW m^{-2})	Reference
CS	Bacterial nanocellulose(BC)	13	~3×10^6	4.8	[119]
SE	BC film+ ZnO nanoparticles,Teflon, ITO glass layers	49.6	4.9	–	[120]
CS	$BaTiO_3$ Composite film/ BC nanofiber, PDMS	181	21	4.8	[121]
CS	PDMS, Cu electrodes BC, $BaTiO_3$, Ag Nanowire	170	9.8	18×10^{-6}	[122]
CS	Au electrodes, CNF film	32.8	35	–	[123]
CS	FEP Allicin-grafted CNF	7.9	5.13	1.01×10^{-7}	[124]
CS	CNF coated with AZO, FEP, $TiCl_4$, Cu electrodes	7	0.7	–	[125]
CS	Phosphorene or Carbon nanofiber	5.2	–	9.36×10^{-7}	[126]
Gear-like CS	PVDF Electrodes, Carbon nanofiber-Ag-PEI	286	4	430	[127]
CS	Teflon ITO electrode Microcrystalline cellulose (MCC)/ PDMS, Al electrodes	28	2.8	64×10^{-7}	[128]
CS	NCC filled PDMS, Aluminum electrodes	320	–	76×10^{-6}	[129]
CS	Aluminum electrodes, EC	245	50	–	[130]
Ridged core	Aluminum electrodes, PI core/ PET/Al	153	3.9	–	[131]
CS	CMF/Ag/CNF, Al plates or MCC	21.9	0.17	76.8×10^{-8}	[132]
CS	CA-PEI, PET or ITO substrate, electrode, FEP	478	–	2.21×10^{-4}	[133]
CS	LTV Conductive fabric CA PTFE	7.3	9.1	–	[134]
CS	317 L SS and Ag electrode EC	45	–	1.2	[135]
CS	PDMS, GO or PCL	120	4	72.5	[136]
CS	Crepe and Cellulose paper, Au electrodes	196.8	31.5	16.1×10^3	[137]
CS	Nitrocellulose film, Ppy-covered cellulose paper, Cupper electrodes.	60	8.8	830	[138]
CS	Cellulose paper, Nitrocellulose film, CNF aerogel	55	0.94	29	[139]
CS	Silver electrodes, PDMS, Cellulose II aerogel	65	1.86	127	[140]
CS	Aluminum electrodes, PTFE, chitosan aerogel, or Cellulose II	242	–	–	[140]
CS	PTFE, Aluminum electrodes, alginic acid aerogel, or Cellulose II	~80	–	–	[140]
CS	PTFE, CMC aerogel or PDMS, Al electrodes	~14	~0.22	–	[141]
CS	PDMS, Cellulose/$BaTiO_3$ aerogel, Kapton, Aluminum electrodes,	48	–	–	[142]
CS	PDMS, Carbon nanofiber/ PEI aerogel, Al electrodes	106.2	9.2	13.3×10^3	[143]
CS	PVDF NF, Wood & Aluminum electrodes	220	5.8	158.2	[144]
CS	Wood, Cupper electrode & PTFE	81	1.8	57	[145]
CS	Cu & Al electrodes, Chitosan-glycerol layer, PTFE	130	~15	–	[146]
CS	Chitosan-acetic acid	~1.6	4×10^{-2}	17.5×10^{-3}	[147]
CS	Kapton, Al electrode Chitosan aerogel, PI, ITO	60.6	7.7	2.33×10^3	[148]
CS	Chitosan-diatom film.	150	1.02	15.7	[149]
SE	Al electrodes, FEP, Ag Nanowire + Chitosan hydrogel + Cu^{2+}	218	–	2×10^3	[150]
CS	PDMS, Chitosan film, PDMS	306	–	–	[151]
CS	Al electrodes Starch film	0.3	–	–	[152]
CS	Cu electrodes, Mixed cellulose ester, $CaCl_2$ + Starch film	1.2	–	170	[153]
CS	PTFE, Thermoplastic starch, Al electrodes.	~560	180	17×10^3	[154]
SE	Carbon tape electrodes, Starch paper	~14	–	–	[155]
CS	Calcium alginate layer, Wire electrode.	33	0.15	–	[156]
CS	Sodium alginate, Al electrodes	1.47	3.9×10^{-3}	3.8	[157]
Cased	Al & Li electrodes, PVA, PVA hydrogel / Alginate+ borax PDMS bag+CaCl2	203.4	17.6	980	[158]
CS	Al electrode, NaF film + Pullulan, Al & Ag electrodes, Kapton	79	–	41.1	[159]
CS	Fish gelatin film, PTFE/PDMS, Cu	130	0.35	46×10^{-7}	[160]
SE	Laver coated silver leaf, rice sheet.	23	0.315	–	[161]

V^*_{oc} = Open circuit voltage, I^*_{sc} = Short circuit current.

plasma drug concentration and area under curves showed an enhancement under elevated temperature conditions. In addition, some drugs (e.g. ethinylestradiol, norelgestromin, etc.) didn't show any significant changes under heat effects [167]. Likewise, using a heating pad in a granisetron TDD system, a slight enhancement in drug flux was observed with no significant changes in the pharmacokinetics of the drug in the human body[168]. The response of the drug not only depends on the body temperature but also on various physiological activities: materials used in drugs, age, hormones, and carrier as well as the structure of the targeted site. Some expert opinion maintains that the body temperature fluctuates in a narrow range and the effects will remain the same. However, researchers found that hypothermia 32º-34º C prolonged response time. The effect of heat due to voltage and current flow should be studied for implantable TENG in regards to drug absorptions, response time, nerve cells, and osteoblast cells.

Future research directions

The material aspect involved in high output TENG fabrication depends on selecting materials from the extreme top end of the triboelectric series. But most of the research is needed to focus on tribo-negative materials (e.g. PTFE, PDMS, and PVDF) because most of the tribo-positive materials are natural or biological materials, such as cotton or human skin. The research found that a significant amount of heloginic groups can enhance electro-negativity [169]. The report showed that fluorinated polymeric sulphur and Al yield a six-fold output voltage raise in comparison with commercial PTFE films [169]. The main drawback of recent tribo-negative material is its electrically insulating behavior that results in the use of other metallic layers in TENG. To address this issue, metallic MXene ($Ti_3C_2T_x$) could be a possible way since it holds high conductivity (~6000–10000 Scm^{-1} with surface terminations (-F) to gain high electronegativity simultaneously [170,171]. Another way to increase the output power of biomechanical motion-driven TENG is through several methods of surface modification (e.g. plasma treatments, chemical treatments, micro/nano structuring of surface topology, etc.), uses of low permittivity substrates, and the introduction of ferroelectric materials with nano-fillers [172]. Dielectric composite contact layers with nanomaterials in an additive physical modification that results in tuning the dielectric constant, managing charge trapping capability, and aligning dipoles which give rise to boost output power, increase pressure response, and lower mechanical modulus [169]. These criteria are important in energy harvesting, TENG-powered electroplating, and self-monitoring. Literature showed that nanoparticles with high permittivity increase dielectric

constant of contact materials. Chen et al. [173] investigated this enhancement effect in PDMS contact layer with some additives like: SiO_2, TiO_2, $BaTiO_3$ and $SrTiO_3$ and found that $SrTiO_3$ yield highest output among these since it has the highest relative permittivity. In another work, Seung et al. [174] showed high- K nanomaterials additives not only increase the dielectric constant but also improve poling effects of PVDF matrix thus decrease the energy level of surface states by employing firm band bending to the composite. It's clear that, adding additives like this increase polarity of the ferroelectric as well as piezoelectric materials and result in increasing output. Future TENG manufacturing needs to add multiple modification technique combined together to increase output and reduce biomechanical energy harvesting hassles.

TENG must be improved in multiple commercial and industrial sectors to compensate for biohazard and in vivo immune toxicity. Poly-saccharide-based TENG could be the possible solution for high-efficiency TENG. Surface properties modification of poly-saccharide could carry out similar triboelectric charge densities in TENG layers that were previously occupied by synthetic polymers. Pan et al. [175] proposed a way to develop fully biodegradable TENG (BD-TENG) using gelatine and PLA films that showed excellent biodegradability. Textile-based TENG is a promising way to harvest biomechanical energy from body movement. DC fabric TENG needed to be prevalent soon due to its cost-effectiveness, uninterrupted electrostatic breakdown phenomena, and wireless power transmission. It will reduce the need for bulky power conversion and management circuits i.e., rectifier bridge or diode. However, its output falls low due to the low level of the surface contact area. Min et al. [176] and Xu et al. [177] showed TENGs output scales with the development of a 'real contact area'. Although contact forces enhance the real contact area, most of the wearables do not have much contact force to press contact layers together. Future research will be employed to develop a well understanding of the particular response to texture at a local scale and the resulting combined response on the global system. Artificial intelligence and deep learning are needed to add to a TENG device for self-monitoring, signal generation, and transmission to the healthcare centre. A feasible animal model should be introduced for more extensive research in the in vivo condition to tactfully handle the immune response, biocompatibility, and inner toxicity environment. Finally, future aspects of TENG will provide an intelligent drug delivery system with sensing feedback and self-regulating drug release under several bodies and environmental conditions, so the development of hybrid TENG is of great significance.

Conclusion

TENGs were frequently used as mechanical energy harvesters in the past few years, but their burgeoning trend can also provide efficient and cost-effective solutions in the field of human motion detection and body energy conversion. TENG-based self-powered systems are used repeatedly in biomedical sensors and IoT-based healthcare systems nowadays. Despite having extensive research in energy harvesting and sensor application, some fields are still untouched. Discussion about one of the emerging technologies like TENG in implantable and electrically supported TDD using electrophoresis, iontophoresis, nanocarrier vehicles, and microneedle-based systems are some sectors that are rarely summarized and need some more research to be conducted. Besides the use of electrical stimuli generated by TENG, it can also expand its application as a thermal heat generator to cause hyperthermia-related cell death. The TENG-driven magnetic field can also be used extensively to drive superparamagnetic nanoparticles in a targeted site. High output TENG can also be exploited fully for IR or light-based delivery which is still rare in practice.

This study summarized self-powered invasive and noninvasive drug delivery systems using wearable or implantable TENGs. The feasibility of TENG developments is also shown in respect of different materials properties since biocompatibility and eco-friendly TENGs are the choice of interest at present. A comprehensive discussion about different biomaterial pairs as dielectric layers of TENGs and their corresponding output voltages, short circuit currents, and power densities are also summarized. Current challenges encountered in today's TENG development are outlined in the discussion section. Some solutions for the causes that impede its progression of being prevalent are given as reference and supposition. This comprehensive summary will provide a pellucid idea and enlighten its reader with some exceptional and untouched fields about TENG-based research.

CRediT authorship contribution statement

P.A., M.A.P.M. conceived the idea. P.A., M.A.P.M. and T.S. discussed the outline and wrote the manuscript. All authors reviewed and approved the manuscript.

Declaration of Competing Interest

The authors declare that they have no known competing financial interests or personal relationships that could have appeared to influence the work reported in this paper.

References

[1] C. Wu, A.C. Wang, W. Ding, H. Guo, Z.L. Wang, Triboelectric nanogenerator: a foundation of the energy for the new era, Adv. Energy Mater. 9 (1) (2019) 1802906.
[2] Z.L. Wang, Triboelectric nanogenerator (TENG)—sparking an energy and sensor revolution, Adv. Energy Mater. 10 (17) (2020) 2000137.
[3] G. Liu, et al., Flexible drug release device powered by triboelectric nanogenerator, Adv. Funct. Mater. 30 (12) (2020) 1909886.
[4] K. Ita, Transdermal iontophoretic drug delivery: advances and challenges, J. Drug Target. 24 (5) (2016) 386–391.
[5] P.C. Pandey, S. Shukla, S.A. Skoog, R.D. Boehm, R.J. Narayan, Current advancements in transdermal biosensing and targeted drug delivery, Sensors 19 (5) (2019) 1028.
[6] Y. Brudno, D.J. Mooney, On-demand drug delivery from local depots, J. Control. Release 219 (2015) 8–17.
[7] C. Padula, G. Colombo, S. Nicoli, P.L. Catellani, G. Massimo, P. Santi, Bioadhesive film for the transdermal delivery of lidocaine: in vitro and in vivo behavior, J. Control. Release 88 (2) (2003) 277–285.
[8] C. Padula, S. Nicoli, S. Pescina, P. Santi, Thin polymeric films for the topical delivery of propranolol, Coll. Surf. B Biointerfaces 174 (2019) 582–586.
[9] L. Engelke, G. Winter, J. Engert, Application of water-soluble polyvinyl alcohol-based film patches on laser microporated skin facilitates intradermal macromolecule and nanoparticle delivery, Eur. J. Pharm. Biopharm. 128 (2018) 119–130.
[10] P. Carter, B. Narasimhan, Q. Wang, Biocompatible nanoparticles and vesicular systems in transdermal drug delivery for various skin diseases, Int. J. Pharm. 555 (2019) 49–62.
[11] L.F. Santos, I.J. Correia, A.S. Silva, J.F. Mano, Biomaterials for drug delivery patches, Eur. J. Pharm. Sci. 118 (2018) 49–66.
[12] I.T. Mendes, A.L.M. Ruela, F.C. Carvalho, J.T.J. Freitas, R. Bonfilio, G.R. Pereira, Development and characterization of nanostructured lipid carrier-based gels for the transdermal delivery of donepezil, Coll. Surf. B Biointerfaces 177 (2019) 274–281.
[13] S.S. Rostamkalaei, J. Akbari, M. Saeedi, K. Morteza-Semnani, A. Nokhodchi, Topical gel of Metformin solid lipid nanoparticles: a hopeful promise as a dermal delivery system, Coll. Surf. B Biointerfaces 175 (2019) 150–157.
[14] J. Zhang, B.B. Michniak-Kohn, Investigation of microemulsion and microemulsion gel formulations for dermal delivery of clotrimazole, Int. J. Pharm. 536 (1) (2018) 345–352.
[15] T.A. Ahmed, M. Khalid, Transdermal film-loaded finasteride microplates to enhance drug skin permeation: two-step optimization study, Eur. J. Pharm. Sci. 88 (2016) 246–256.
[16] M. Contardi, et al., Transparent ciprofloxacin-povidone antibiotic films and nanofiber mats as a potential skin and wound care dressings, Eur. J. Pharm. Sci. 104 (2017) 133–144.
[17] I. Aranaz, R. Harris, F. Navarro-García, A. Heras, N. Acosta, Chitosan based films as supports for dual antimicrobial release, Carbohydr. Polym. 146 (2016) 402–410.

[18] S. Patel, S. Srivastava, M.R. Singh, D. Singh, Preparation and optimization of chitosan-gelatin films for sustained delivery of lupeol for wound healing, Int. J. Biol. Macromol. 107 (2018) 1888–1897.
[19] S. Mura, J. Nicolas, P. Couvreur, Stimuli-responsive nanocarriers for drug delivery, Nat. Mater. 12 (11) (2013) 991–1003.
[20] R. Langer, Drug delivery and targeting, Nature 392 (6679 Suppl) (1998) 5–10.
[21] W.J. Dower, J.F. Miller, C.W. Ragsdale, High-efficiency transformation of E. coli by high voltage electroporation, Nucleic Acids Res. 16 (13) (1988) 6127–6145.
[22] R. Yang, T. Wei, H. Goldberg, W. Wang, K. Cullion, D.S. Kohane, Getting drugs across biological barriers, Adv. Mater. 29 (37) (2017) 1606596.
[23] Y.N. Kalia, A. Naik, J. Garrison, R.H. Guy, Iontophoretic drug delivery, Adv. Drug Deliv. Rev. 56 (5) (2004) 619–658.
[24] Y.T. Yi, J.Y. Sun, Y.W. Lu, Y.C. Liao, Programmable and on-demand drug release using electrical stimulation, Biomicrofluidics 9 (2) (2015) 22401.
[25] K. Ita, Transdermal delivery of heparin: physical enhancement techniques, Int. J. Pharm. 496 (2) (2015) 240–249.
[26] M. Sanromán-Iglesias, K.A.I. Zhang, A. Chuvilin, C.H. Lawrie, M. Grzelczak, L.M. Liz-Marzán, Conjugated polymers as molecular gates for light-controlled release of gold nanoparticles, ACS Appl. Mater. Interfaces 7 (29) (2015) 15692–15695.
[27] R.C. Smith, M. Riollano, A. Leung, P.T. Hammond, Layer-by-layer platform technology for small-molecule delivery, Angew. Chem. 121 (47) (2009) 9136–9139.
[28] J. Hong, B.-S. Kim, K. Char, P.T. Hammond, Inherent charge-shifting polyelectrolyte multilayer blends: a facile route for tunable protein release from surfaces, Biomacromolecules 12 (8) (2011) 2975–2981.
[29] M. Bok, et al., Microneedles integrated with a triboelectric nanogenerator: an electrically active drug delivery system, Nanoscale 10 (28) (2018) 13502–13510.
[30] A.-R. Denet, V. Preat, Transdermal delivery of timolol by electroporation through human skin, J. Control. Release 88 (2) (2003) 253–262.
[31] S.-L. Chang, G.A. Hofmann, L. Zhang, L.J. Deftos, A.K. Banga, The effect of electroporation on iontophoretic transdermal delivery of calcium regulating hormones, J. Control. Release 66 (2–3) (2000) 127–133.
[32] B.M. Medi, J. Singh, Electronically facilitated transdermal delivery of human parathyroid hormone (1–34), Int. J. Pharm. 263 (1–2) (2003) 25–33.
[33] S. Guo, A. Donate, G. Basu, C. Lundberg, L. Heller, R. Heller, Electro-gene transfer to the skin using a noninvasive multielectrode array, J. Control. Release 151 (3) (2011) 256–262.
[34] Y. Tokudome, K. Sugibayashi, The effects of calcium chloride and sodium chloride on the electroporation-mediated skin permeation of fluorescein isothiocyanate (FITC)-dextrans in vitro, Biol. Pharm. Bull. 26 (10) (2003) 1508–1510.
[35] Q. Ouyang, et al., Self-powered, on-demand transdermal drug delivery system driven by triboelectric nanogenerator, Nano Energy 62 (2019) 610–619.
[36] A. Jadoul, J. Bouwstra, V. Preat, Effects of iontophoresis and electroporation on the stratum corneum: a review of the biophysical studies, Adv. Drug Deliv. Rev. 35 (1) (1999) 89–105.
[37] F.-R. Fan, Z.-Q. Tian, Z.L. Wang, Flexible triboelectric generator, Nano Energy 1 (2) (2012) 328–334.
[38] L. Zhou, D. Liu, J. Wang, Z.L. Wang, Triboelectric nanogenerators: fundamental physics and potential applications, Friction 8 (3) (2020) 481–506.
[39] H. Feng, C. Zhao, P. Tan, R. Liu, X. Chen, Z. Li, Nanogenerator for biomedical applications, Adv. Healthc. Mater. 7 (10) (2018) 1701298.
[40] G. Khandelwal, N.P.M.J. Raj, S.-J. Kim, Triboelectric nanogenerator for healthcare and biomedical applications, Nano Today 33 (2020) 100882.
[41] Z.L. Wang, On Maxwell's displacement current for energy and sensors: the origin of nanogenerators, Mater. Today 20 (2) (2017) 74–82.
[42] Z.L. Wang, A.C. Wang, On the origin of contact-electrification, Mater. Today 30 (2019) 34–51.
[43] C. Xu, et al., On the electron-transfer mechanism in the contact-electrification effect, Adv. Mater. 30 (15) (2018) 1706790.
[44] J. Lowell, A.R. Akande, Contact electrification-why is it variable? J. Phys. D Appl. Phys. 21 (1) (1988) 125.
[45] Z.L. Wang, On the first principle theory of nanogenerators from Maxwell's equations, Nano Energy 68 (2020) 104272.
[46] S. Niu, Z.L. Wang, Theoretical systems of triboelectric nanogenerators, Nano Energy 14 (2015) 161–192.
[47] R. Hinchet, W. Seung, S. Kim, Recent progress on flexible triboelectric nanogenerators for self-powered electronics, ChemSusChem 8 (14) (2015) 2327–2344.
[48] A. Chen, C. Zhang, G. Zhu, Z.L. Wang, Polymer materials for high-performance triboelectric nanogenerators, Adv. Sci. 7 (14) (2020) 2000186.
[49] S. Pan, Z. Zhang, Fundamental theories and basic principles of triboelectric effect: a review, Friction 7 (1) (2019) 2–17, https://doi.org/10.1007/s40544-018-0217-7
[50] Z.L. Wang, Triboelectric nanogenerators as new energy technology and self-powered sensors–principles, problems, and perspectives, Faraday Discuss. 176 (2015) 447–458.
[51] G. Zhu, et al., Triboelectric-generator-driven pulse electrodeposition for micropatterning, Nano Lett. 12 (9) (2012) 4960–4965.
[52] S. Niu, et al., Theory of sliding-mode triboelectric nanogenerators, Adv. Mater. 25 (43) (2013) 6184–6193.
[53] S. Niu, et al., A theoretical study of grating structured triboelectric nanogenerators, Energy Environ. Sci. 7 (7) (2014) 2339–2349.
[54] G. Zhu, et al., A shape-adaptive thin-film-based approach for 50% high-efficiency energy generation through micro-grating sliding electrification, Adv. Mater. 26 (23) (2014) 3788–3796.
[55] L. Lin, Y. Xie, S. Niu, S. Wang, P.-K. Yang, Z.L. Wang, Robust triboelectric nanogenerator based on rolling electrification and electrostatic induction at an instantaneous energy conversion efficiency of~ 55%, ACS Nano 9 (1) (2015) 922–930.
[56] S. Jung, J. Lee, T. Hyeon, M. Lee, D. Kim, Fabric-based integrated energy devices for wearable activity monitors, Adv. Mater. 26 (36) (2014) 6329–6334.
[57] W. Liu, M. Han, X. Sun, B. Meng, X.-S. Zhang, H. Zhang, An unmovable single-layer triboelectric generator driven by sliding friction, Nano Energy 9 (2014) 401–407.
[58] C. Wu, et al., Self-powered iontophoretic transdermal drug delivery system driven and regulated by biomechanical motions, Adv. Funct. Mater. 30 (3) (2020) 1907378.
[59] B. Meng, et al., A transparent single-friction-surface triboelectric generator and self-powered touch sensor, Energy Environ. Sci. 6 (11) (2013) 3235–3240.
[60] G. Zhu, et al., Self-powered, ultrasensitive, flexible tactile sensors based on contact electrification, Nano Lett. 14 (6) (2014) 3208–3213.
[61] S. Niu, et al., Theoretical investigation and structural optimization of single-electrode triboelectric nanogenerators, Adv. Funct. Mater. 24 (22) (2014) 3332–3340.
[62] W. Yang, et al., Triboelectrification based motion sensor for human-machine interfacing, ACS Appl. Mater. Interfaces 6 (10) (2014) 7479–7484.
[63] B. Meng, X. Cheng, X. Zhang, M. Han, W. Liu, H. Zhang, Single-friction-surface triboelectric generator with human body conduit, Appl. Phys. Lett. 104 (10) (2014) 103904.
[64] Z.L. Wang, L. Lin, J. Chen, S. Niu, Y. Zi, Triboelectric nanogenerator: single-electrode mode, Triboelectric Nanogenerators, Springer, 2016, pp. 91–107.
[65] S. Wang, Y. Xie, S. Niu, L. Lin, Z.L. Wang, Freestanding triboelectric-layer-based nanogenerators for harvesting energy from a moving object or human motion in contact and non-contact modes, Adv. Mater. 26 (18) (2014) 2818–2824.
[66] J. Chen, Z.L. Wang, Reviving vibration energy harvesting and self-powered sensing by a triboelectric nanogenerator, Joule 1 (3) (2017) 480–521.
[67] Z. Liu, H. Li, B. Shi, Y. Fan, Z.L. Wang, Z. Li, Wearable and implantable triboelectric nanogenerators, Adv. Funct. Mater. 29 (20) (2019) 1808820.
[68] Y. Zi, S. Niu, J. Wang, Z. Wen, W. Tang, Z.L. Wang, Standards and figure-of-merits for quantifying the performance of triboelectric nanogenerators, Nat. Commun. 6 (1) (2015) 1–8.
[69] J. Hadgraft, R.H. Guy, Transdermal drug delivery: developmental issues and research initiatives, Drugs Pharm. Sci. 35 (1989).
[70] A. Williams, Transdermal and Topical Drug Delivery from Theory to Clinical Practice, Pharmaceutical Press, 2003.
[71] M.R. Prausnitz, S. Mitragotri, R. Langer, Current status and future potential of transdermal drug delivery, Nat. Rev. Drug Discov. 3 (2) (2004) 115–124.
[72] R.L. Bronaugh, H.I. Maibach, Percutaneous Absorption: Drugs–Cosmetics–Mechanisms–Methodology: Drugs–Cosmetics–Mechanisms–Methodology, CRC Press, 1999.
[73] W.Y. Jeong, M. Kwon, H.E. Choi, K.S. Kim, Recent advances in transdermal drug delivery systems: a review, Biomater. Res. 25 (1) (2021) 24.
[74] M. Foldvari, S. Babiuk, I. Badea, DNA delivery for vaccination and therapeutics through the skin, Curr. Drug Deliv. 3 (1) (2006) 17–28.
[75] A. Sieg, R.H. Guy, M.B. Delgado-Charro, Noninvasive and minimally invasive methods for transdermal glucose monitoring, Diabetes Technol. Ther. 7 (1) (2005) 174–197.
[76] M.J. Garland, E. Caffarel–Salvador, K. Migalska, A.D. Woolfson, R.F. Donnelly, Dissolving polymeric microneedle arrays for electrically assisted transdermal drug delivery, J. Control. Release 159 (1) (2012) 52–59.
[77] G.M. Gelfuso, et al., Iontophoresis enhances voriconazole antifungal potency and corneal penetration, Int. J. Pharm. 576 (2020) 118991.
[78] N.D. Singh, A.K. Banga, Controlled delivery of ropinirole hydrochloride through the skin using modulated iontophoresis and microneedles, J. Drug Target. 21 (4) (2013) 354–366.
[79] H. Patel, A. Joshi, A. Joshi, G. Stagni, Effect of microporation on passive and iontophoretic delivery of diclofenac sodium, Drug Dev. Ind. Pharm. 41 (12) (2015) 1962–1967.
[80] V. Kumar, A.K. Banga, Modulated iontophoretic delivery of small and large molecules through microchannels, Int. J. Pharm. 434 (1–2) (2012) 106–114.
[81] N.K. Andanooru Chandrappa, B. Channakeshavaiah Ravikumar, S.M. Rangegowda, Iontophoretic delivery of methotrexate in the treatment of palmar psoriasis: a randomised controlled study, Australas. J. Dermatol. 61 (2) (2020) 140–146.
[82] S. Kwon, et al., Electrodeless reverse electrodialysis patches as an ionic power source for active transdermal drug delivery, Adv. Funct. Mater. 28 (15) (2018) 1705952.
[83] S. Katikaneni, A. Badkar, S. Nema, A.K. Banga, Molecular charge mediated transport of a 13 kD protein across microporated skin, Int. J. Pharm. 378 (1–2) (2009) 93–100.
[84] C.S. Ivanoff, et al., AC electrokinetic drug delivery in dentistry using an interdigitated electrode assembly powered by inductive coupling, Biomed. Microdev. 18 (5) (2016) 1–14.
[85] S.S.S. Lanke, C.S. Kolli, J.G. Strom, A.K. Banga, Enhanced transdermal delivery of low molecular weight heparin by barrier perturbation, Int. J. Pharm. 365 (1–2) (2009) 26–33.

[86] J. Yang, et al., Smartphone-powered iontophoresis-microneedle array patch for controlled transdermal delivery, Microsyst. Nanoeng. 6 (1) (2020) 112, https://doi.org/10.1038/s41378-020-00224-z
[87] Y. Wang, L. Zeng, W. Song, J. Liu, Influencing factors and drug application of iontophoresis in transdermal drug delivery: an overview of recent progress, Drug Deliv. Transl. Res. (2021).
[88] D. Park, H. Park, J. Seo, S. Lee, Sonophoresis in transdermal drug delivery, Ultrasonics 54 (1) (2014) 56–65.
[89] K. Ita, Recent progress in transdermal sonophoresis, Pharm. Dev. Technol. 22 (4) (2017) 458–466.
[90] H. Feiszthuber, S. Bhatnagar, M. Gyöngy, C.-C. Coussios, Cavitation-enhanced delivery of insulin in agar and porcine models of human skin, Phys. Med. Biol. 60 (6) (2015) 2421.
[91] Z. Yu, Y. Liang, W. Liang, Low-frequency sonophoresis enhances rivastigmine permeation in vitro and in vivo, Die Pharm. Int. J. Pharm. Sci. 70 (6) (2015) 379–380.
[92] M. Bok, Z.-J. Zhao, S. Jeon, J.-H. Jeong, E. Lim, Ultrasonically and iontophoretically enhanced drug-delivery system based on dissolving microneedle patches, Sci. Rep. 10 (1) (2020) 2027.
[93] B. Zorec, S. Becker, M. Reberšek, D. Miklavčič, N. Pavšelj, Skin electroporation for transdermal drug delivery: the influence of the order of different square wave electric pulses, Int. J. Pharm. 457 (1) (2013) 214–223.
[94] Z. Liu, et al., Self-powered intracellular drug delivery by a biomechanical energy-driven triboelectric nanogenerator, Adv. Mater. 31 (12) (2019) 1807795.
[95] Y. Wang, et al., Poking cells for efficient vector-free intracellular delivery, Nat. Commun. 5 (1) (2014) 1–9.
[96] M. Bok, et al., Microneedles integrated with a triboelectric nanogenerator: an electrically active drug delivery system, Nanoscale 10 (28) (2018) 13502–13510.
[97] C. Chiappini, Nanoneedle-based sensing in biological systems, ACS Sens. 2 (8) (2017) 1086–1102.
[98] L. Xu, Y. Yang, Y. Mao, Z. Li, Self-powerbility in electrical stimulation drug delivery system, Adv. Mater. Technol. (2021) 2100055.
[99] B. Pamornpathomkul, S. Duangjit, S. Laohapatarapant, T. Rojanarata, P. Opanasopit, T. Ngawhirunpat, Transdermal delivery of fluorescein isothiocyanate-dextrans using the combination of microneedles and low-frequency sonophoresis, Asian J. Pharm. Sci. 10 (5) (2015) 415–424.
[100] S. Tokumoto, N. Higo, H. Todo, K. Sugibayashi, Effect of combination of low-frequency sonophoresis or electroporation with iontophoresis on the mannitol flux or electroosmosis through excised skin, Biol. Pharm. Bull. 39 (7) (2016) 1206–1210.
[101] M. Petchsangsai, T. Rojanarata, P. Opanasopit, T. Ngawhirunpat, The combination of microneedles with electroporation and sonophoresis to enhance hydrophilic macromolecule skin penetration, Biol. Pharm. Bull. (2014) b14–00321.
[102] M. Amjadi, S. Sheykhansari, B.J. Nelson, M. Sitti, Recent advances in wearable transdermal delivery systems, Adv. Mater. 30 (7) (2018) 1704530.
[103] J.-P. Sylvestre, R.H. Guy, M.B. Delgado-Charro, In vitro optimization of dexamethasone phosphate delivery by iontophoresis, Phys. Ther. 88 (10) (2008) 1177–1185.
[104] J. Ge, E. Neofytou, T.J. Cahill III, R.E. Beygui, R.N. Zare, Drug release from electric-field-responsive nanoparticles, ACS Nano 6 (1) (2012) 227–233.
[105] S. Sirivisoot, R. Pareta, T.J. Webster, Electrically controlled drug release from nanostructured polypyrrole coated on titanium, Nanotechnology 22 (8) (2011) 85101.
[106] M.W.J. Prins, W.J.J. Welters, J.W. Weekamp, Fluid control in multichannel structures by electrocapillary pressure, Science 291 (5502) (2001) 277–280.
[107] R.A. Hayes, B.J. Feenstra, Video-speed electronic paper based on electrowetting, Nature 425 (6956) (2003) 383–385.
[108] A. Garaventa, et al., A phase II study of topotecan with vincristine and doxorubicin in children with recurrent/refractory neuroblastoma, Cancer 98 (11) (2003) 2488–2494.
[109] J. Zhu, et al., Recombinant human interleukin-1 receptor antagonist protects mice against acute doxorubicin-induced cardiotoxicity, Eur. J. Pharmacol. 643 (2–3) (2010) 247–253.
[110] C. Chen, W. Xu, C. Wang, Combination of celecoxib and doxorubicin increases growth inhibition and apoptosis in acute myeloid leukemia cells, Leuk. Lymphoma 54 (11) (2013) 2517–2522.
[111] C. Zhao, et al., Highly efficient in vivo cancer therapy by an implantable magnet triboelectric nanogenerator, Adv. Funct. Mater. 29 (41) (2019) 1808640.
[112] Y. Feng, X. Huang, S. Liu, W. Guo, Y. Li, H. Wu, A self-powered smart safety belt enabled by triboelectric nanogenerators for driving status monitoring, Nano Energy 62 (2019) 197–204.
[113] Y. Yang, et al., Liquid-metal-based super-stretchable and structure-designable triboelectric nanogenerator for wearable electronics, ACS Nano 12 (2) (2018) 2027–2034.
[114] Y. Jie, Q. Jiang, Y. Zhang, N. Wang, X. Cao, A structural bionic design: from electric organs to systematic triboelectric generators, Nano Energy 27 (2016) 554–560.
[115] Q. Zheng, et al., In vivo self-powered wireless cardiac monitoring via implantable triboelectric nanogenerator, ACS Nano 10 (7) (2016) 6510–6518.
[116] F. Arab Hassani, et al., Toward self-control systems for neurogenic underactive bladder: a triboelectric nanogenerator sensor integrated with a bistable micro-actuator, ACS Nano 12 (4) (2018) 3487–3501.
[117] J. Wang, H. Wang, N.V. Thakor, C. Lee, Self-powered direct muscle stimulation using a triboelectric nanogenerator (TENG) integrated with a flexible multiple-channel intramuscular electrode, ACS Nano 13 (3) (2019) 3589–3599.
[118] M.A. Parvez Mahmud, N. Huda, S.H. Farjana, M. Asadnia, C. Lang, Recent advances in nanogenerator-driven self-powered implantable biomedical devices, Adv. Energy Mater. 8 (2) (2018) 1701210.
[119] H.-J. Kim, E.-C. Yim, J.-H. Kim, S.-J. Kim, J.-Y. Park, I.-K. Oh, Bacterial nano--cellulose triboelectric nanogenerator, Nano Energy 33 (2017) 130–137.
[120] S. Jakmuangpak, T. Prada, W. Mongkolthanaruk, V. Harnchana, S. Pinitsoontorn, Engineering bacterial cellulose films by nanocomposite approach and surface modification for biocompatible triboelectric nanogenerator, ACS Appl. Electron. Mater. 2 (8) (2020) 2498–2506.
[121] Y. Shao, C. Feng, B. Deng, B. Yin, M. Yang, Facile method to enhance output performance of bacterial cellulose nanofiber-based triboelectric nanogenerator by controlling micro-nano structure and dielectric constant, Nano Energy 62 (2019) 620–627.
[122] H. Oh, et al., Highly conductive ferroelectric cellulose composite papers for efficient triboelectric nanogenerators, Adv. Funct. Mater. 29 (37) (2019) 1904066.
[123] C. Yao, A. Hernandez, Y. Yu, Z. Cai, X. Wang, Triboelectric nanogenerators and power-boards from cellulose nanofibrils and recycled materials, Nano Energy 30 (2016) 103–108.
[124] S. Roy, H.-U. Ko, P.K. Maji, J. Kim, Large amplification of triboelectric property by allicin to develop high performance cellulosic triboelectric nanogenerator, Chem. Eng. J. 385 (2020) 123723.
[125] B. Yang, C. Yao, Y. Yu, Z. Li, X. Wang, Nature degradable, flexible, and transparent conductive substrates from green and earth-abundant materials, Sci. Rep. 7 (1) (2017) 1–8.
[126] P. Cui, K. Parida, M. Lin, J. Xiong, G. Cai, P.S. Lee, Transparent, flexible cellulose nanofibril–phosphorene hybrid paper as a triboelectric nanogenerator, Adv. Mater. Interfaces 4 (22) (2017) 1700651.
[127] C. Zhang, et al., Chemically functionalized cellulose nanofibrils-based gear-like triboelectric nanogenerator for energy harvesting and sensing, Nano Energy 66 (2019) 104126.
[128] A. Chandrasekhar, N.R. Alluri, B. Saravanakumar, S. Selvarajan, S.-J. Kim, A microcrystalline cellulose ingrained polydimethylsiloxane triboelectric nanogenerator as a self-powered locomotion detector, J. Mater. Chem. C 5 (7) (2017) 1810–1815.
[129] J. Peng, et al., A composite generator film impregnated with cellulose nanocrystals for enhanced triboelectric performance, Nanoscale 9 (4) (2017) 1428–1433.
[130] M. Wang, W. Li, C. You, Q. Wang, X. Zeng, M. Chen, Triboelectric nanogenerator based on 317L stainless steel and ethyl cellulose for biomedical applications, RSC Adv. 7 (11) (2017) 6772–6779.
[131] A.S.M.I. Uddin, G.-S. Chung, Wide-ranging impact-competent self-powered active sensor using a stacked corrugated-core sandwich-structured robust triboelectric nanogenerator, Sens. Actuators B Chem. 245 (2017) 1–10.
[132] X. He, et al., A hierarchically nanostructured cellulose fiber-based triboelectric nanogenerator for self-powered healthcare products, Adv. Funct. Mater. 28 (45) (2018) 1805540.
[133] Z. Bai, et al., Highly flexible, porous electroactive biocomposite as attractive tribopositive material for advancing high-performance triboelectric nanogenerator, Nano Energy 75 (2020) 104884.
[134] S.R. Srither, D.S. Shankar Rao, S. Krishna Prasad, Triboelectric nanogenerator based on biocompatible and easily available polymer films, ChemistrySelect 3 (18) (2018) 5055–5061.
[135] A. Šutka, et al., Triboelectric nanogenerator based on immersion precipitation derived highly porous ethylcellulose, J. Electrostat. 92 (2018) 1–5.
[136] S. Parandeh, M. Kharaziha, F. Karimzadeh, An eco-friendly triboelectric hybrid nanogenerators based on graphene oxide incorporated polycaprolactone fibers and cellulose paper, Nano Energy 59 (2019) 412–421.
[137] S. Chen, J. Jiang, F. Xu, S. Gong, Crepe cellulose paper and nitrocellulose membrane-based triboelectric nanogenerators for energy harvesting and self-powered human-machine interaction, Nano Energy 61 (2019) 69–77.
[138] X. Shi, S. Chen, H. Zhang, J. Jiang, Z. Ma, S. Gong, Portable self-charging power system via integration of a flexible paper-based triboelectric nanogenerator and supercapacitor, ACS Sustain. Chem. Eng. 7 (22) (2019) 18657–18666.
[139] C. Qian, et al., All-printed 3D hierarchically structured cellulose aerogel based triboelectric nanogenerator for multi-functional sensors, Nano Energy 63 (2019) 103885.
[140] L. Zhang, et al., Cellulose II aerogel-based triboelectric nanogenerator, Adv. Funct. Mater. 30 (28) (2020) 2001763.
[141] M. Beyranvand, A. Gholizadeh, Facile and low-cost synthesis of flexible nanogenerators based on polymeric and porous aerogel materials, Curr. Appl. Phys. 20 (1) (2020) 226–231.
[142] K. Shi, X. Huang, B. Sun, Z. Wu, J. He, P. Jiang, Cellulose/BaTiO3 aerogel paper-based flexible piezoelectric nanogenerators and the electric coupling with triboelectricity, Nano Energy 57 (2019) 450–458.
[143] H.-Y. Mi, et al., High-performance flexible triboelectric nanogenerator based on porous aerogels and electrospun nanofibers for energy harvesting and sensitive self-powered sensing, Nano Energy 48 (2018) 327–336.
[144] S. Hao, J. Jiao, Y. Chen, Z.L. Wang, X. Cao, Natural wood-based triboelectric nanogenerator as self-powered sensing for smart homes and floors, Nano Energy 75 (2020) 104957.
[145] J. Luo, et al., Flexible and durable wood-based triboelectric nanogenerators for self-powered sensing in athletic big data analytics, Nat. Commun. 10 (1) (2019) 1–9.

[146] Y.-T. Jao, et al., A textile-based triboelectric nanogenerator with humidity-resistant output characteristic and its applications in self-powered healthcare sensors, Nano Energy 50 (2018) 513–520.
[147] R. Wang, et al., Engineered and laser-processed chitosan biopolymers for sustainable and biodegradable triboelectric power generation, Adv. Mater. 30 (11) (2018) 1706267.
[148] Q. Zheng, et al., Highly porous polymer aerogel film-based triboelectric nanogenerators, Adv. Funct. Mater. 28 (13) (2018) 1706365.
[149] J.-N. Kim, et al., Skin-attachable and biofriendly chitosan-diatom triboelectric nanogenerator, Nano Energy 75 (2020) 104904.
[150] L. Wang, W.A. Daoud, Hybrid conductive hydrogels for washable human motion energy harvester and self-powered temperature-stress dual sensor, Nano Energy 66 (2019) 104080.
[151] Z. Yu, et al., Rapidly fabricated triboelectric nanogenerator employing insoluble and infusible biomass materials by fused deposition modeling, Nano Energy 68 (2020) 104382.
[152] R. Ccorahua, A. Cordero, C. Luyo, M. Quintana, E. Vela, Starch-cellulose-based triboelectric nanogenerator obtained by a low-cost cleanroom-free processing method, MRS Adv. 4 (23) (2019) 1315–1320.
[153] R. Ccorahua, J. Huaroto, C. Luyo, M. Quintana, E.A. Vela, Enhanced-performance bio-triboelectric nanogenerator based on starch polymer electrolyte obtained by a cleanroom-free processing method, Nano Energy 59 (2019) 610–618.
[154] P.K. Sarkar, T. Kamilya, S. Acharya, Introduction of triboelectric positive bioplastic for powering portable electronics and self-powered gait sensor, ACS Appl. Energy Mater. 2 (8) (2019) 5507–5514.
[155] Z. Zhu, K. Xia, Z. Xu, H. Lou, H. Zhang, Starch paper-based triboelectric nanogenerator for human perspiration sensing, Nanoscale Res. Lett. 13 (1) (2018) 1–6.
[156] Y. Pang, F. Xi, J. Luo, G. Liu, T. Guo, C. Zhang, An alginate film-based degradable triboelectric nanogenerator, RSC Adv. 8 (12) (2018) 6719–6726.
[157] Q. Liang, et al., Recyclable and green triboelectric nanogenerator, Adv. Mater. 29 (5) (2017) 1604961.
[158] X. Jing, et al., Enhancing the performance of a stretchable and transparent triboelectric nanogenerator by optimizing the hydrogel ionic electrode property, ACS Appl. Mater. Interfaces 12 (20) (2020) 23474–23483.
[159] Y. Lu, X. Li, J. Ping, J. He, J. Wu, A flexible, recyclable, and high-performance pullulan-based triboelectric nanogenerator (TENG), Adv. Mater. Technol. 5 (2) (2020) 1900905.
[160] X. Zhang, et al., Sustainable and transparent fish gelatin films for flexible electroluminescent devices, ACS Nano 14 (4) (2020) 3876–3884.
[161] G. Khandelwal, et al., All edible materials derived biocompatible and biodegradable triboelectric nanogenerator, Nano Energy 65 (2019) 104016.
[162] C. Zhao, X. Cui, Y. Wu, Z. Li, Recent progress of nanogenerators acting as self-powered drug delivery devices, Adv. Sustain. Syst. 5 (4) (2021) 2000268.
[163] F.P. Schmook, J.G. Meingassner, A. Billich, Comparison of human skin or epidermis models with human and animal skin in in-vitro percutaneous absorption, Int. J. Pharm. 215 (1–2) (2001) 51–56.
[164] J.E. Seto, B.E. Polat, R.F.V. Lopez, D. Blankschtein, R. Langer, Effects of ultrasound and sodium lauryl sulfate on the transdermal delivery of hydrophilic permeants: comparative in vitro studies with full-thickness and split-thickness pig and human skin, J. Control. Release 145 (1) (2010) 26–32.
[165] N. Sekkat, Y.N. Kalia, R.H. Guy, Biophysical study of porcine ear skin in vitro and its comparison to human skin in vivo, J. Pharm. Sci. 91 (11) (2002) 2376–2381.
[166] J. Hao, P. Ghosh, S.K. Li, B. Newman, G.B. Kasting, S.G. Raney, Heat effects on drug delivery across human skin, Expert Opin. Drug Deliv. 13 (5) (2016) 755–768.
[167] L.S. Abrams, et al., Pharmacokinetics of norelgestromin and ethinyl estradiol delivered by a contraceptive patch (Ortho EvraTM/EvraTM) under conditions of heat, humidity, and exercise, J. Clin. Pharmacol. 41 (12) (2001) 1301–1309.
[168] S.T. Haislip, J.W. Gilmore, J.D. Howell, Results from four pharmacokinetic studies of the granisetron transdermal system, Res. Rep. Transdermal Drug Deliv. 2 (2013) 19–26.
[169] Y. Zhou, W. Deng, J. Xu, J. Chen, Engineering materials at the nanoscale for triboelectric nanogenerators, Cell Rep. Phys. Sci. (2020) 100142.
[170] Y. Dong, et al., Metallic MXenes: a new family of materials for flexible triboelectric nanogenerators, Nano Energy 44 (2018) 103–110.
[171] B. Anasori, Û.G. Gogotsi, 2D Metal Carbides and Nitrides (MXenes), Springer, 2019.
[172] R. Walden, C. Kumar, D.M. Mulvihill, S.C. Pillai, Opportunities and challenges in triboelectric nanogenerator (TENG) based sustainable energy generation technologies: a mini-review, Chem. Eng. J. Adv. (2021) 100237.
[173] J. Chen, et al., Enhancing performance of triboelectric nanogenerator by filling high dielectric nanoparticles into sponge PDMS film, ACS Appl. Mater. Interfaces 8 (1) (. 2016) 736–744.
[174] W. Seung, et al., Boosting power-generating performance of triboelectric nanogenerators via artificial control of ferroelectric polarization and dielectric properties, Adv. Energy Mater. 7 (2) (2017) 1600988.
[175] R. Pan, et al., Fully biodegradable triboelectric nanogenerators based on electrospun polylactic acid and nanostructured gelatin films, Nano Energy 45 (2018) 193–202.
[176] G. Min, Y. Xu, P. Cochran, N. Gadegaard, D.M. Mulvihill, R. Dahiya, Origin of the contact force-dependent response of triboelectric nanogenerators, Nano Energy 83 (2021) 105829.
[177] Y. Xu, G. Min, N. Gadegaard, R. Dahiya, D.M. Mulvihill, A unified contact force-dependent model for triboelectric nanogenerators accounting for surface roughness, Nano Energy 76 (2020) 105067.

Partho Adhikary received his B.Sc. degree in Biomedical Engineering from Khulna University of Engineering & Technology, Bangladesh. During his undergraduate years, he researched composite materials and polymer chemistry and published one journal paper on expanded perlite-based composite materials. He is ardently looking for RA or TA position to pursue his PhD degree in cutting-edge research in biomaterials for tissue engineering, drug delivery, biosensor, and nanofabrication. He is an information geek who finds his predilection in arts, literature, music, and sports besides his STEM subjects.

Dr. M A Parvez Mahmud (Member, IEEE) is currently the Alfred Deakin Postdoctoral Fellow of the School of Engineering, Deakin University, Melbourne, VIC, Australia. After the successful completion of his PhD degree in Engineering with several awards, he worked as a Postdoctoral Research Associate and Academic in the School of Engineering at Macquarie University, Sydney. He has made significant research contributions in the area of energy sustainability, energy harvesting, artificial intelligence, and smart sensing, and published more than 130 scholarly articles, including 2 authored books, 9 book chapters, 87 peer-reviewed journal articles, and 39 fully refereed conference proceedings.

Tahsin Solaiman received his B.Sc. in biomedical engineering from Khulna University of Engineering & Technology, Bangladesh, where he is currently pursuing a master's degree. His current research interests include biosensors, biomaterials, drug delivery, nanofabrication, and mathematical modeling. He has published a research article in IEEE Sensors Journal and presented a paper on biomaterials for drug delivery at the conference, ICMIEE in December 2018. Besides, he has participated in a range of national and international seminars and workshops focusing on diverse fields of biomedical. He acted as the role of Joint Secretary of Bioinformatics and Artificial Intelligence Club, KUET.

Zhong Lin Wang Hightower Chair in Materials Science and Engineering and Regents' Professor at Georgia Tech, the Chief Scientist and Director of the Beijing Institute of Nanoenergy and Nanosystems, Chinese Academy of Sciences. His discovery and breakthroughs in developing nanogenerators and self-powered nanosystems establish the principle and technological roadmap for harvesting mechanical energy from environmental and biological systems for powering personal electronics and future sensor networks. He coined and pioneered the field of piezotronics and piezophototronics.